Characterization of Spin Coated Polymers in Nano-environments as a Function of Film Thickness

Catherine E. Beck

Thesis submitted to the Faculty of the
Virginia Polytechnic Institute and State University
in partial fulfillment for the requirements for the degree of

Master of Science
in
Chemistry

Thomas C. Ward, Chair
Alan R. Esker
John G. Dillard

July 26, 2001
Blacksburg, VA

Keywords: Thin films, Cooperativity, Polymer Brushes

Characterization of Spin Coated Polymers in Nano-environments
as a Function of Film Thickness
(Abstract)

Catherine E. Beck

Polymer applications have become more demanding as industry continuously turns to more microscopic parts. Due to the interactions of the polymer chains with the supporting surface and the air interface, the thinner films required for such applications have distinctly different properties than those of the well-defined bulk systems. The goal of the current research is to elucidate the behavior of ultrathin films. Two separate studies were performed on thin films supported on silicon wafer substrates: the first focuses on the viscoelastic cooperativity of thin films, and the second concentrates on the morphological behavior of polymer brush films.

For the first study, polymethyl methacrylate films were spin coated onto silicon wafers, and the film thickness was determined using ellipsometry. A series of thin films were examined using techniques such as dielectric analysis and thermal mechanical analysis. The theory of cooperativity, which explains polymeric behavior using the intermolecular and intramolecular forces among polymer chains, was employed to understand the behavior of these thin films.

Another type of thin film, a polymer brush, was investigated in the second study. Polymer brushes are formed by chemically bonding one end of many polymer chains to a substrate. The other ends of the chains can interact with the surrounding environment creating a brush-like structure. Constraining one end of a polymer chain alters the behavior of such a thin film. Polymer brushes of the di-block copolymer poly(*t*-butyl methacrylate) and polystyrene were produced on silicon wafers using spin coating techniques. The effects of both grafting density and solvent washes were analyzed using contact angle analysis and atomic force microscopy. In addition, hydrolysis was successfully performed on existing polymer brush samples to produce polymer brushes of the di-block copolymer polymethyl acrylic acid and polystyrene.

Table of Contents

1 Chapter I Introduction 1
2 Chapter II Literature Review 2
2.1 Cooperativity 2
2.2 Thin Films 5
2.3 Spin Coating 8
2.4 Ellipsometry 10
2.5 Dielectric Analysis 11
2.6 Thermal Mechanical Analysis 12
2.7 Polymer Brushes 12
2.8 Contact Angles 16
2.9 Atomic Force Microscopy 17
3 Chapter III Experimental 19
3.1 Cooperativity Studies 19
3.2 Polymer Brush Studies 22
4 Chapter IV Results and Discussion: Cooperativity Studies 27
4.1 Differential Scanning Calorimetry 27
4.2 Gel Permeation Chromatography 28
4.3 Ellipsometry 29
4.4 Dielectric Analysis 32
4.5 Thermal Mechanical Analysis 36
4.6 Summary of Cooperativity Studies 39
5 Chapter V Results and Discussion: Polymer Brush Studies 40
5.1 Contact Angles 40
5.2 X-ray Photoelectron Spectroscopy 42
5.3 Ellipsometry 47
5.4 Atomic Force Microscopy 48
5.5 Summary of Polymer Brush Studies 70

List of Figures

Figure 2.1-1: Temperature dependence of the shift factor for several polymers 4
Figure 2.2-1: Substrate-polymer interactions of PMMA on silicon. 7
Figure 2.2-2: Change of T_g with film thickness. 8
Figure 2.3-1: Stages of spin coating 9
Figure 2.7-1: Polymer brush chain conformations. 13
Figure 2.7-2: Brush height versus grafting amount for homopolymers (R_g = radius of gyration). 14
Figure 2.7-3: Brush height versus grafting density for di-block copolymers. 14
Figure 2.7-4: Polymer brush self-assembly of a di-block copolymer. 15
Figure 2.8-1: Contact Angle Analysis 16
Figure 3.1-1: Schematic of Dielectric Instrument 21
Figure 3.2-1: Chemical structure of di-block copolymer. 22
Figure 4.1-1: DSC scan of PMMA (Endotherm Up) 27
Figure 4.2-1: GPC results for PMMA 28
Figure 4.3-1: Film Thickness versus Spin Speed for each sample 30
Figure 4.3-2: Film thickness vs. solution concentration for the 3000 rpm samples 31
Figure 4.4-1: DEA results for clean silicon wafer, permittivity as temperature increased 32
Figure 4.4-2: DEA of clean silicon wafer 33
Figure 4.4-3: DEA results of 50 nm PMMA film on silicon 34
Figure 4.4-4: DEA results of a second 50 nm film sample on silicon 35
Figure 4.4-5: DEA results of a second clean silicon wafer sample 36
Figure 4.5-1: 900 nm DMA 37
Figure 4.5-2: TMA results of 50 nm film of PMMA, no apparent transition 38
Figure 4.5-3: TMA results of 660 nm film superimposed on blank silicon wafer 39
Figure 5.1-1: Contact angles of water on copolymer brush samples. 41
Figure 5.2-1: XPS elemental analysis of oxygen on 20t sample 45
Figure 5.2-2: XPS elemental analysis of oxygen on 20ht sample 45
Figure 5.2-3: XPS elemental analysis of carbon on 20t sample 46
Figure 5.2-4: XPS elemental analysis of carbon on 20ht sample 46
Figure 5.4-1: AFM image of a clean silicon wafer. 49

Figure 5.4-2: 3-D AFM image of a clean silicon wafer..... 49
Figure 5.4-3: AFM image of 40t sample after 10 hours of toluene wash..... 50
Figure 5.4-4: AFM image of 100t sample after 10 hours of toluene wash..... 51
Figure 5.4-5: AFM images of 10t sample..... 52
Figure 5.4-6: 3-D AFM image of 10t sample. 52
Figure 5.4-7: AFM images of 20t sample..... 53
Figure 5.4-8: 3-D AFM image of 20t sample. 53
Figure 5.4-9: AFM images of 40t sample..... 54
Figure 5.4-10: 3-D AFM image of 40t sample. 54
Figure 5.4-11: AFM images of 100t sample..... 55
Figure 5.4-12: 3-D AFM image of 100t sample. 55
Figure 5.4-13: AFM images of 40ht sample..... 57
Figure 5.4-14: 3-D AFM image of 40ht sample. 57
Figure 5.4-15: AFM images of 100ht sample..... 58
Figure 5.4-16: 3-D AFM image of 100ht sample. 58
Figure 5.4-17: AFM images of 100c sample. 59
Figure 5.4-18: 3-D AFM image of 100c sample..... 59
Figure 5.4-19: AFM images of 100hc sample. 60
Figure 5.4-20: 3-D AFM image of 100hc sample..... 60
Figure 5.4-21: Summary chart of the average height difference for each polymer brush sample. 62
Figure 5.4-22: Height analysis of AFM image for 10t sample..... 63
Figure 5.4-23: Height analysis of AFM image for 20t sample..... 64
Figure 5.4-24: Height analysis of AFM image for 40t sample..... 65
Figure 5.4-25: Height analysis of AFM image for 100t sample..... 66
Figure 5.4-26: Height analysis of AFM image for 40ht sample..... 67
Figure 5.4-27: Height analysis of AFM image for 100ht sample..... 68
Figure 5.4-28: Height analysis of AFM image for 100c sample. 69
Figure 5.4-29: Height analysis of AFM image for 100hc sample. 70

List of Tables

Table 2.1-1: Coupling parameters of several polymers. 3
Table 2.8-1: Contact angle results for polymethacrylates. 17
Table 4.3-1: Film Thickness and error for 2% PMMA solution..... 29
Table 4.3-2: Film Thickness and error for 5% PMMA solution..... 29
Table 4.3-3: Film Thickness and error for 10% PMMA solution..... 29
Table 5.1-1: Contact angles for methylene iodide. 42
Table 5.1-2: Surface energy with dispersive and polar components. 42
Table 5.2-1: XPS results (15°), atomic concentration table for one measurement of 20ht sample. 43
Table 5.2-2: XPS results (90°), atomic concentration table for one measurement of 20ht sample. 43
Table 5.2-3: XPS results (15°), atomic concentration table for one measurement of 20t sample. 44
Table 5.2-4: XPS results (90°), atomic concentration table for one measurement of 20t sample. 44
Table 5.3-1: Di-block sample film thickness from ellipsometry after 10 hours of washing 47
Table 5.3-2: Di-block sample film thickness from ellipsometry after 34 hours of washing 48

1 Chapter I
Introduction

This thesis describes the behavior of ultrathin polymer films supported on a silicon wafer substrate. Two separate studies have been performed: the first focuses on the viscoelastic cooperativity of thin films, and the second concentrates on the morphological behavior of polymer brush films.

Industrial use of thin films has increased for several reasons including the development of ever-smaller electronic devices. As applications of polymers become smaller and thinner, the behavior of polymer chains in these confined geometries needs to be understood. Many aspects need to be probed such as the effect of molecular weight, thermal degradation, and the adhesion properties. In the first study, one characterization scheme, cooperativity, was chosen to summarize the influence of the small scale on polymer behavior. The theory of cooperativity focuses on polymer chain interactions and relates those interactions to macroscopic behavior. This research looks specifically at the well-defined system of polymethyl methacrylate and silicon to understand better how cooperativity reveals polymeric behavior in thin films.

The second study focuses on a new type of thin film, polymer brushes. By chemically bonding one end of many polymer chains to a substrate, leaving the other ends free to interact with a second environment, one can create a brush-like structure. The constraints placed on these polymer chains produce a range of morphological behavior depending on a number of factors. When exposed to different solvents, the chain conformations are variable. This thesis reports the effects of chemical composition and variable solvents on di-block copolymer brushes.

2 Chapter II

Literature Review

2.1 Cooperativity

2.1.1 Cooperative Motion

Unlike simple molecules, polymers have a distribution of relaxation times. This non-exponential nature of the relaxation functions of polymers has led to the development of many theories to model their behavior, especially near the glass transition. In 1965, Adam and Gibbs stated that polymer relaxations occur via groups of molecules which rearrange cooperatively.[1] This idea of cooperative relaxation was an important move towards defining the role of polymer interaction in relaxation phenomena.

More recently, Angell developed a theory describing the 'fragility' of a system.[2] Fragile liquids experienced structural degradation as the temperature of the system increases above the glass transition. Conversely, strong liquids held onto their structural integrity longer due to their network structures. Ngai and Plazek extended these concepts of intermolecular and intramolecular forces to polymeric behavior with the introduction of the coupling model.[3] This model depicted the relaxation of macromolecules as many individual segmental relaxations. But, such local relaxations must involve the molecules in the surrounding environment through coupling interactions among the polymer chains. These interactions depended on the amount of intermolecular and intramolecular forces, or the cooperativity, of the polymer. A coupling parameter, n, was also defined in the model to give a quantitative measure of the cooperativity. It ranged from a value of 0 for materials that experienced little coupling to 1 for materials that demonstrated more coupling or a higher cooperativity. In addition, the coupling model relates the coupling parameter to the breadth of the relaxation distribution- the higher the coupling parameter or cooperativity, the broader the relaxation times for the polymer. Because of their mutual emphasis on interactions within and between molecules, the concept of fragility and the coupling model are closely related.

Due to the dependence of cooperativity on intermolecular interactions, chemical structure pays a large role in the coupling parameter. Ngai and Roland have explored the effect of chemical structure on the cooperativity of polymers.[4] An increase of intermolecular forces, such as dipoles or hydrogen bonding, can amplify the cooperativity of the system. Ngai's results are summarized in a table of coupling parameters calculated for different polymers. An excerpt of these results appears in Table 2.1-1.

Table 2.1-1: Coupling parameters of several polymers.[5]

Glass Former	n = 1-β (at T_g)
Polybutadiene 1,2	0.74
Polycarbonate (BPA-PC)	0.65
Poly(methylmethacrylate)	0.63
Polybutadiene 1,4	0.58
Poly(vinylacetate)	0.52
Polyisoprene	0.50

2.1.2 Cooperative Analysis

Ngai and Plazek developed a relationship between the "primitive relaxation times," τ_o, and the measured relaxation times, τ^*.[6] Because τ_o was dependent on both temperature and molecular weight, the relaxation times were related to the coupling parameter, n, where ω_c is a coupling crossover frequency.

$$\tau^* = \left[(1-n)\omega_c^n \tau_o\right]^{1/(1-n)} \qquad (1)$$

The relationship of a_T, explained as a ratio of relaxation times

$$a_T = \tau^*(T)/\tau^*(T_R) \qquad (2)$$

where T_R is a reference temperature and T is the temperature of the measurement, was applied to Equation 1. This ratio gave the following equation after substitution.

$$(1-n)\log a_T = (1-n)\log\frac{\tau^*(T)}{\tau^*(T_R)} = \log\frac{\tau_o(T)}{\tau_o(T_R)} \qquad (3)$$

In Ngai and Plazek's publications, they determined that numerous sets of data could be reconciled with the well known Williams-Landel-Ferry Equation.[6] If the glass transition temperature (T_g) was utilized as the reference temperature, then:

$$(1-n)\log a_T = \frac{-C_1(T-T_g)/T_g}{C_2+(T-T_g)/T_g} \qquad (4)$$

The empirical parameters C_1 and C_2 were calculated to be 5.49 and 0.141 respectively and can be used to determine n.

In addition to the numerical values, the free-standing, neat polymer systems were also compared using cooperativity plots. These plots place log a_T on the y-axis and $(T-T_g)/T_g$ on the x-axis. For these graphs, a steeper slope reflects a higher coupling parameter. A series of polymers is represented by such a plot in Figure 2.1-1.

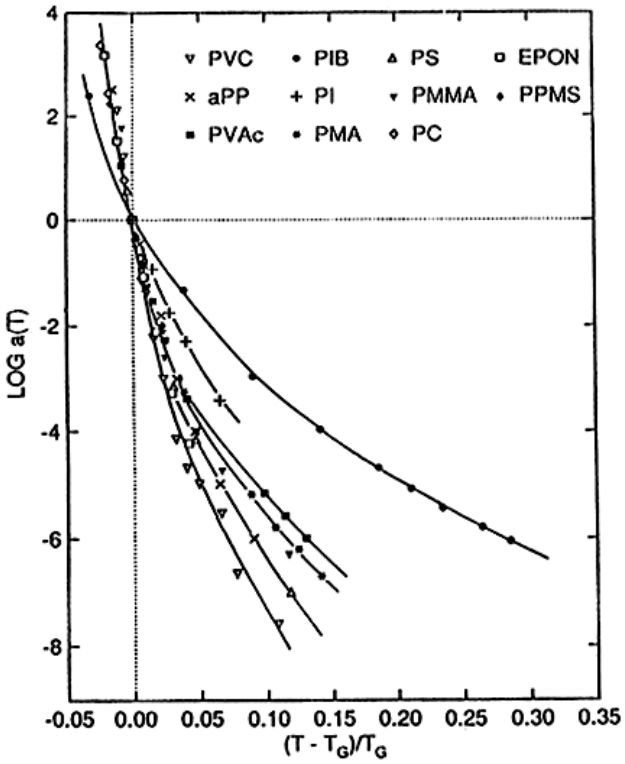

Figure 2.1-1: Temperature dependence of the shift factor for several polymers[6]

2.2 Thin Films

Many bulk polymer properties have been well defined in the recent literature.[7] In addition, theories that offer reasoning for changes in these bulk properties with temperature, pressure, etc. have been developed. Focus has been shifted in the past decade to polymers in thin film geometries. These systems remain obscure to polymer scientists.

Thin films have become ubiquitous in the polymer industry. Fueled by the microelectronics industry and its need for miniature parts, polymer applications have become more demanding. Polymers in these environments have been tested and modeled in laboratories around the world: from universities to automobile companies, research surrounding thin films is quickly growing.[8]

Two main areas of research have emerged that cover thin polymer films. The first, free-standing films, investigates thin films unattached to a substrate. The main concern in this field is how the air-polymer interface affects the behavior of the polymer as the film decreases in thickness. The second, polymer films on substrates, focuses on the interactions at the polymer-substrate interface. Both research fields have reported data and offered explanations for what has been observed. Although the second area is more relevant to the current research, the two interrelate, so the literature for each appears below.

2.2.1 Free-Standing Films

The major difference in bulk polymer properties and those of a thin, free-standing film is the proximity of the polymer-air interface. The mobility of the polymer chains at this interface is an important concern to applications such as adhesion, melt pressing, and latex film formation.[9] This mobility also affects the glass transition temperature (T_g), a prominent property of polymers. In general, as the film thickness decreases, the T_g also decreases - as much as 60°C in free-standing films. Ngai explains this decrease using the coupling model.[10] His paper cites two factors that contribute to the lower transition temperature. First, as the film thickness approaches the average end-to-end distance,

induced orientation can occur in the film. Of course, this condition applies mostly for ultrathin films of high molecular weight polymers. Second, the polymer chains that are near the surface of the polymer have a higher mobility (or what Ngai calls a decrease in the "cooperative length scale."[10]) The chains near the surface interact with proportionally less polymer chains than those in the center. Their coupling parameter decreases due to fewer interactions, mobility increases, and therefore, the depression in T_g is observed. Here, Ngai provides a crucial link of the glass transition temperature as a measure of the cooperativity of the polymer. Of course, a measured T_g represents some ensemble average of "surface" and "bulk" polymer.

Although useful for modeling, most thin film applications are not free-standing, but confined to a substrate. These confined geometries present new challenges as the effects of more than one interface must be considered.

2.2.2 Polymer Films on Substrates

Current research has focused on the task of defining thin film behavior when the polymer is cast on a surface. Although the theories developed for free-standing films apply to the free surface of the system, the effect of the substrate on polymer properties needed to be investigated. Keddie et al. observed polymethyl methacrylate (PMMA) on two different substrates, the native oxide of silicon and gold evaporated onto silicon.[9] The two systems produced drastically different results as measured by spectroscopic ellipsometry. As the polymer film thickness decreased, the PMMA on the gold surface showed a decrease in the T_g whereas the PMMA on the silicon surface showed an increase at the same thickness. Keddie argued that PMMA does not have a favorable interaction with gold; therefore the effect of the polymer-air interface would dominate the mobility of the polymer and result in the change in T_g. Conversely, hydrogen bonding can occur between the hydroxyl groups of the silicon surface and the oxygen in PMMA as seen in Figure 2.2-1. In this system, the substrate interactions would dominate the behavior of the polymer. Wallace used similar reasoning stating that the interactions with the surface could act as a crosslink in the polymer by restraining certain chains.[11] For thin films, those less than approximately 60 nm, significant increases in T_g could occur.

These researchers saw shifts of as much as 60°C. Van Zanten chose a different polymer, poly-(2)- vinyl pyridine, to cast on silicon.[12] This polymer should interact more strongly with the silicon than PMMA and also show an increase in T_g . Indeed transition temperatures increased anywhere from 20°C to 50°C above the bulk T_g as observed by x-ray reflectometry. In addition, these researchers calculated that the effects of the surface extended several hundreds of angstroms into the polymer.[12]

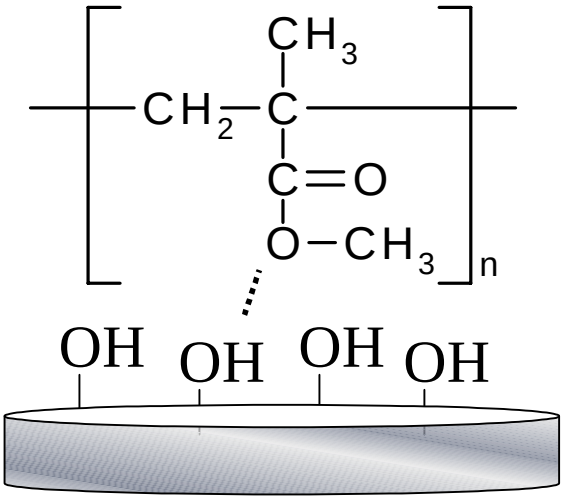

Figure 2.2-1: Substrate-polymer interactions of PMMA on silicon.

Thin films on substrates provide a characterization challenge: the whole system must be measured at once and substrate properties can easily mask those of the thin film. Other techniques have been employed to study these complex systems. Fryer et al. used local thermal analysis to probe polystyrene (PS) and PMMA on two different substrates.[13] These results were comparable to ellipsometry values establishing local thermal analysis as an effective technique. Again, PS did not have a favorable interaction with the polar or nonpolar silicon surface and both PS systems showed a decrease in T_g with decreasing film thickness. PMMA showed similar behavior on the nonpolar surface. However, on the polar substrate the T_g increased as the PMMA films became thinner. Porter saw similar effects measuring PMMA on silica with a differential scanning

calorimeter (DSC).[14] The DSC showed an increase of 50°C above the bulk T_g for films of 0.6 Å.

An excellent summary is provided by a macromolecular simulation done by Torres et al.[15] Using hard spheres as polymer models and programming desired polymer-interface interactions, the group was able to duplicate selected experimental results. Their data for a free-standing film, a polymer-interface weak interaction, and a polymer-interface strong interaction can be seen in Figure 2.2-2. This research aids in understanding the behavior of thin polymer films. Free-standing films have increased mobility at two surfaces, a decreased coupling parameter, and therefore lower T_g's as the films become thinner. For films with weak substrate-polymer interactions, the T_g also dropped although not as sharply since these films only have one free surface. Inversely, polymer-substrate interactions that are strong produce an increased cooperativity and therefore a higher T_g as films become thinner.

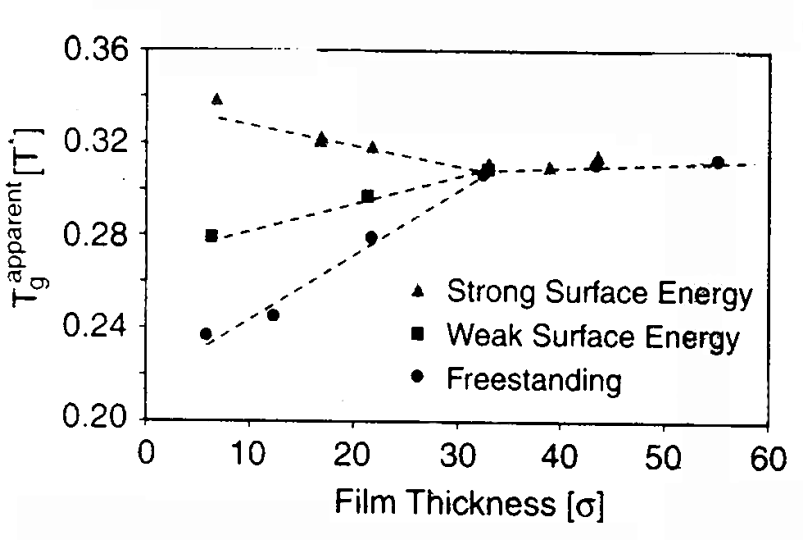

Figure 2.2-2: Change of T_g with film thickness.

2.3 Spin Coating

Many techniques needed to be developed to create and monitor these new thin film systems. An accurate method for producing thin polymer films was the first objective of this thesis research. The proposed solution to the problem was spin coating. First a polymer solution was made and was pipetted onto the desired surface. Next, the

substrate was "accelerated to a desired rotation rate."[16] Spinning continued until an equilibrium film thickness was reached. This was followed by annealing to alleviate radial orientation and eliminate any remaining solvent.

Several variables can control the film thickness of the final product. Extrand looked at some of the experimental parameters in spin coating.[17] The solvent used to make the solution does affect the final thickness of the film. Different viscosity and solubility can make PMMA films cast from a cyclohexane solution twice as thick as those cast from a toluene solution.[17] The research also showed that thickness increased as spin speed decreased as would be expected. The amount of solution applied to the wafer did not affect the thickness as long as there was enough present to cover the surface. Any excess was simply flung off the surface by centripetal forces.

Because thin films are used in so many applications, Bornside, Macosko, and Scriven developed a model for achieving a desired film thickness.[18] They divided spin coating into the four stages of deposition, spin-up, spin-off, and evaporation (Figure 2.3-1). By taking both the force of spinning and the concentration-controlled evaporation into account, these researchers were able to predict film thickness. This model was extremely useful because it included the surface chemistry and the type of polymer used. Because of the dependable nature of the method and the ease of use, spin coating is frequently used to create polymer thin films.

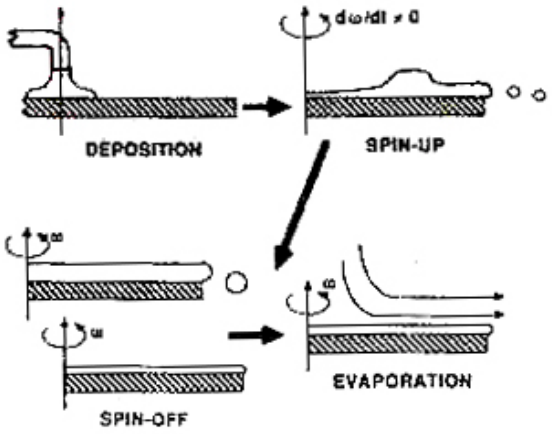

Figure 2.3-1: Stages of spin coating [18]

2.4 Ellipsometry

2.4.1 Theory

Ellipsometry uses polarized light to analyze optical properties of diverse samples. The linearly polarized light is reflected off the sample surface. Data are taken across an area of the surface and averaged to give a more accurate representation of the properties for the entire film. For a spectroscopic ellipsometers, a range of light from 350 nm to 1000 nm is used to acquire a spectrum. After reflection, the light becomes elliptically polarized. The analyzer measures the orientation and the direction of the reflected light. From these values, the phase change, Δ, and the amplitude change, ψ, can be calculated.[19] When working with a known polymer, its index of refraction is required to allow for a fitting of the actual film thickness.

2.4.2 Applications

The recent interest in thin film research has been aided by more refined ellipsometers and their characterization ability. Initially, the instrument was employed to find the film thickness of static samples.[17,20] The data was expanded to include the index of refraction for known and unknown polymers.[21] New developments then turned to heating stages to measure the dynamic properties of thin films. As the sample was heated, the change in film thickness could be monitored. Similar to dilatometry data, the expansion plotted against temperature gave a change in slope at the T_g. Many groups began acquiring transition temperatures with this method.[9,13] With the ability to calculate T_g of the whole system, the ellipsometer became an indispensable tool in thin film characterization.

2.5 Dielectric Analysis

2.5.1 Theory

Dielectric Analysis (DEA) is used to measure the loss modulus, storage modulus, and thus temperature transitions of polymers. Specifically, DEA studies the motion of the polymer chain. As the sample is placed into the electric field produced by the instrument, polar polymer chains react by orienting along the field. This polarity mainly arises from polar bonds in the chain or from polar side groups. Low temperature transitions can be assigned to side chain motion, usually involving rotations via DEA. High temperature transitions manifest larger, whole chain motion. These transitions are indicative of the T_g.[22] In addition, DEA can measure these polymer motions over a wide range of frequencies: 10^{-5} to 10^{9} Hz.[23] This ability makes DEA a powerful characterization technique, particularly when time-temperature superposition is applied.[24] By recording the response of the polymer chains to the electric field, the dielectric permittivity, loss, and cooperativity of the polymer can be measured.

2.5.2 Applications

Dielectric analysis of bulk polymer properties has been well documented.[22] Similarly, DEA has often been employed in monitoring polymer reactions.[22] Another, quite common application uses DEA to measure the breadth of a polymer relaxation.[25] This analysis is directly related to the coupling parameter, which quantifies cooperativity. DEA has been used for characterizing thin polymer films.[8] However, the polymer systems that have been studied involve free-standing films that have been sputter coated on both sides. Adding conductive substrates, such as aluminum foil, has also been accomplished,[8] as well as relying on sputter coated, conducting surfaces.

2.6 Thermal Mechanical Analysis

2.6.1 Theory

Thermal mechanical analysis can be used to assess the glass transition of a thin film system. The sample is placed in a temperature-controlled chamber for analysis. Two different probes can be used with thermal mechanical analysis (TMA): a flat probe or a penetration probe.[26] The flat probe measures the thermal expansion of the polymer as the temperature is increased. Very little load is applied, so an accurate measure of change in dimension can be reported. Conversely, the penetration probe can have up to 1.0 N of force placed on the sample. The probe pushes into the sample as it softens to give a crude modulus (or compliance) value or a temperature associated with a transition.[26]

2.6.2 Applications

For bulk polymers, both the coefficient of thermal expansion and the modulus have been measured as mentioned above.[26] A more sensitive procedure has been developed for thin film analysis called local thermal analysis (LTA). In this technique the probe itself is heated and is therefore able to measure the expansion and transitions of thin films more accurately.[13]

2.7 Polymer Brushes

An advancement in thin film polymers has appeared in the last 20 years. By chemically bonding one end of many polymer chains to a substrate, a monolayer of polymer chains can be manufactured. By tethering one end of a polymer chain to the surface, its motion is restricted. Several chain conformations have been proposed such as the mushrooms and clusters as seen in Figure 2.7-1.

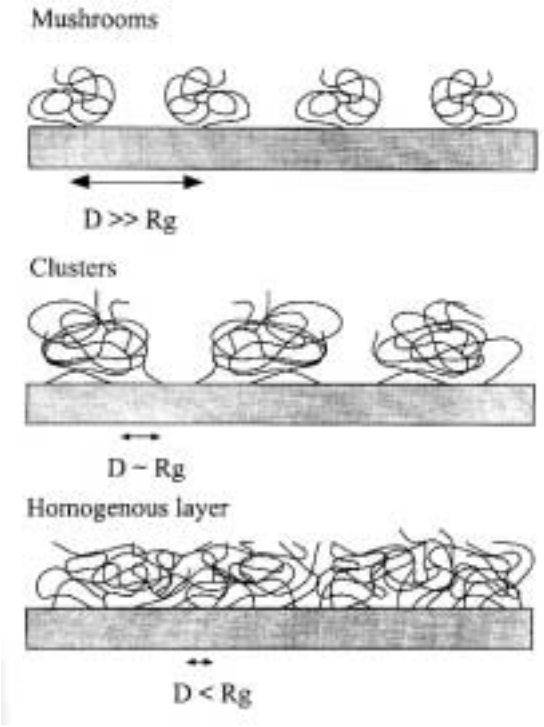

Figure 2.7-1: Polymer brush chain conformations.[27]

The number of chains bonded to a given area of the substrate is known as the grafting density. As this density increases, intermolecular crowding forces the chains to take on stretched conformations, or a longer end-to-end distance, which differs from the characteristic random-walk of a free polymer. Therefore, increasing the surface concentration of polymer chains leads to an increase in film thickness or height (h). This relationship between grafting density and polymer brush height can be seen in both homopolymers (Figure 2.7-2) and di-block copolymers (Figure 2.7-3).

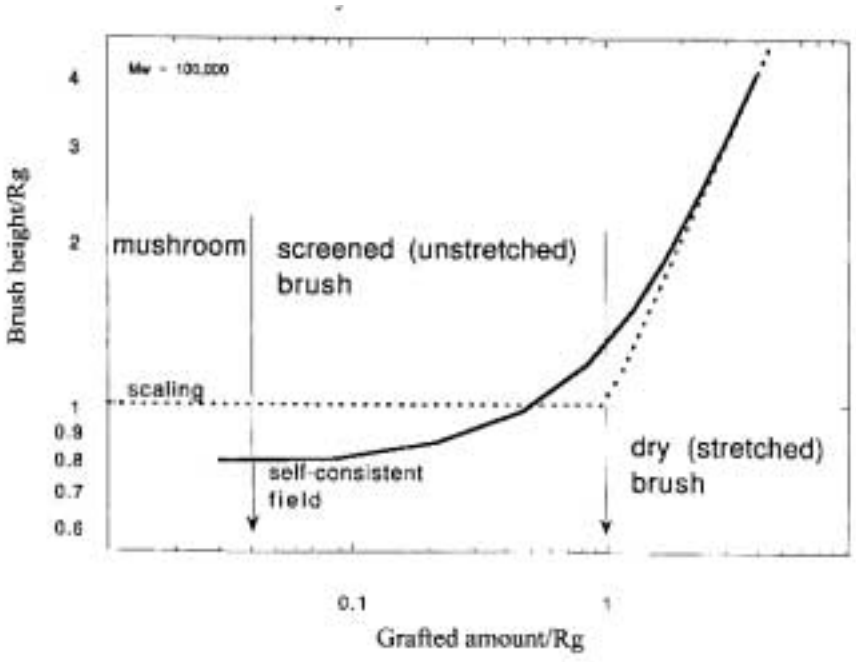

Figure 2.7-2: Brush height versus grafting amount for homopolymers (R_g = radius of gyration).[27]

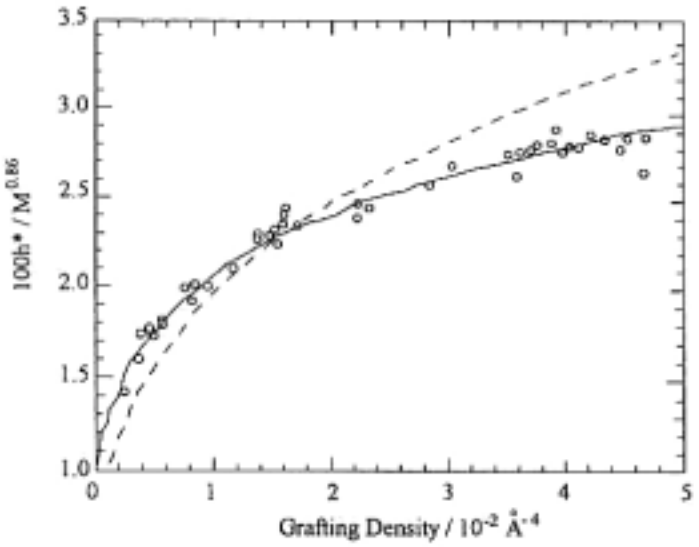

Figure 2.7-3: Brush height versus grafting density for di-block copolymers.[27]

The stretched polymer configuration changes the film mechanical properties as well as the film morphology. The polymer film thickness that ultimately occurs is a result of a complex balance of free energy factors.[28] The usual random-walk conformation must compete with the desire of the polymer to stretch out in a good solvent. Because of these competing forces, it is not unusual for the height of the film to be greater than the radius of gyration for the polymer.

Diblock copolymers can also exhibit self-assembled layers. Although the first chain is grafted to the substrate, subsequent chains can assemble in stacked layers by alternating their orientation. In other words, the A-block can be bonded to the surface leaving the B-block at the air (or solvent) interface; the next chain can place the B-block down to favorably interact with the first B-block, and leave the A-block up and so on, alternating layers. An illustration of this self-assembly is shown in Figure 2.7-4.

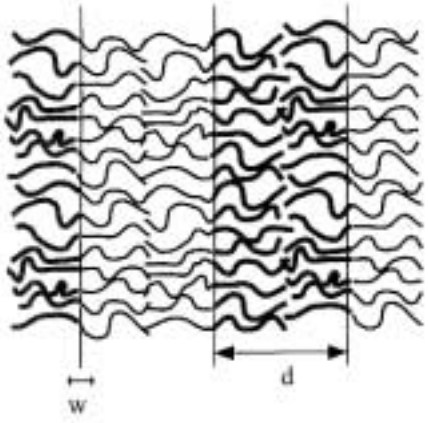

Figure 2.7-4: Polymer brush self-assembly of a di-block copolymer.[27]

Many characterization techniques for polymer brushes such as light scattering, nuclear magnetic resonance, atomic force microscopy, and contact angle measurements appear in the literature.[28] Previous papers have demonstrated morphological differences due to the molecular weight of polymer chains[28] and even differences caused by the last solvent used to wash the brush.[29] The work of Zhao, et al. showed brush morphologies changing from smooth, after washing in CH_2Cl_2, to a worm-like structure and then to a hemispherical shape as cyclohexane was slowly added to the wash solution.[29] Changing

the solvent composition by as little as 10 % induced drastic contrast in polymer brush behavior. Previous work by Wang, et al.[30] has been continued in this present thesis research to understand better the morphological changes due to grafting density and solvent washes.

2.8 Contact Angles

2.8.1 Theory

By measuring the contact angle between a solid surface and a free-standing liquid drop, the relative energetics between the two can be evaluated. For example, if a drop of water beads up on a substrate, then the surface likely has nonpolar or hydrophobic characteristics. Conversely, if water wets the substrate, then the surface is more likely polar or hydrophilic. Figure 2.8-1 illustrates the definition of the contact angle (θ) and the relevant surface energy values.

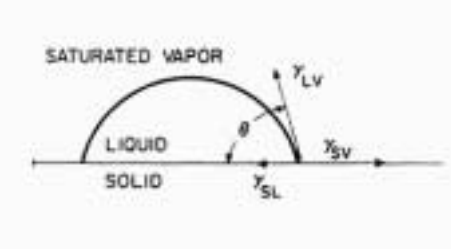

Figure 2.8-1: Contact Angle Analysis [31]

In addition to this simple characterization, by measuring the contact angle using two different liquids, the solid surface energy can be calculated. This total energy (γ) is often decomposed into the sum of polar (γ^p) and dispersive (γ^d) components. Using the measured contact angle and published surface energy values for water and methylene iodide, a form of Young's Equation can be solved simultaneously to obtain surface energy values.[31]

$$(1+\cos\theta_1)\gamma_1 = 4\left(\frac{\gamma_1^d\gamma_s^d}{\gamma_1^d+\gamma_s^d}+\frac{\gamma_1^p\gamma_s^p}{\gamma_1^p+\gamma_s^p}\right) \quad (5)$$

$$(1+\cos\theta_2)\gamma_2 = 4\left(\frac{\gamma_2^d\gamma_s^d}{\gamma_2^d+\gamma_s^d}+\frac{\gamma_2^p\gamma_s^p}{\gamma_2^p+\gamma_s^p}\right) \quad (6)$$

2.8.2 Applications

Contact angles give a macroscopic picture of the surface. This technique quickly assesses surface properties for applications such as adhesion and wetting.[31] In molecular terms, specific backbone or side chain compositions have been examined by contact angle analysis. Wulf, et al. looked at the influence of the side chain groups in polyalkyl methacrylates.[32] Their conclusions showed a gradual increase of the contact angle of water and a decrease of the polymer surface energy as the side group increased in size or bulk. Some of the results for poly*t*-butyl methacrylate (P*t*BMA), poly*n*-butyl metharylate (P*n*BMA), and polymethyl methacrylate (PMMA) can be viewed in Table 2.8-1.[32]

Table 2.8-1: Contact angle results for polymethacrylates.

θw (PMMA)[31]	80°	γ_{sv}(PMMA)[32]	38.5 ± 0.5 dyne/cm
θw (P*n*BMA)[31]	91°	γ_{sv} (P*n*BMA)[32]	28.8 ± 0.5 dyne/cm
θw (P*t*BMA)[32]	108.08° ± 0.53	γ_{sv} (P*t*BMA)[32]	18.1 ± 0.6 dyne/cm

2.9 Atomic Force Microscopy

2.9.1 Theory

Atomic force microscopy (AFM) maps out the topographical features of a surface. A miniature tip (radius of curvature is 5-10 nm[40]), usually made of silicon or silicon nitride, taps along a prescribed area of the surface being imaged.[33] Attractive and repulsive electrostatic forces affect the motion of the tip as it operates close to the surface. A piezoelectric scanning actuator works in a feedback loop to raise or lower the

cantilever beam that holds the tip, thus maintaining constant amplitude of oscillation as the surface height changes. A laser beam records the deflection of the cantilever beam as the tip rasters along the surface. Typically a height image, monitoring relative elevation, and a phase image, analogous to relative modulus, are produced.

2.9.2 Applications

Many different surface measurements can be done on a microscopic scale using AFM. In the tapping mode described above, phase images show the well-defined boundaries of phase separations. Height images give a topographical map of the surface. Both the height and phase image can be used together to create a complete picture of the surface morphology. Also, tips can be used in the more destructive contact mode to measure friction or adhesion by dragging along the surface.

3 Chapter III
Experimental

3.1 Cooperativity Studies

3.1.1 Material

It has been demonstrated that chemical structure directly affects cooperativity.[34] To simplify the research, one amorphous polymer with a high molecular weight was chosen. Polymethyl methacrylate (PMMA) was purchased from Aldrich in the powder form. Gel permeation chromatography showed a Mw of 101,300 g/mol with a polydispersity of 1.967.

3.1.2 Sample Preparation

3.1.2.1 Surface Treatment

Polished silicon wafers one inch in diameter and ~0.30 mm thick were purchased from Wafer World, Inc. The wafers were held isothermally at 90°C for 90 minutes in a 30/70 solution by volume of H_2O_2 and H_2SO_4 respectively.[35] Next, they were submersed in acetone in a sonicator for 30 minutes. The wafers were then rinsed with acetone and dried in a stream of air. This treatment produced a native oxide layer on the silicon wafers that were used as the substrate for depositing thin films of PMMA.

3.1.2.2 Spin Coating

Solutions of PMMA in toluene were prepared at 2%, 5%, and 10% by weight. The silicon wafers were positioned on the spin coater and several drops of solution were placed on the wafer. Immediately, each sample began rotating at a constant speed to

acquire the desired film thickness. These speeds ranged from 1250 to 3000 rpm to produce film thicknesses from 50 to 900 nm. The samples were spun for one minute and then heated in a vacuum oven at 165°C for 24 hours. Because the samples were heated 65°C above the glass transition temperature of the polymer, any remaining toluene (boiling point, 110.6°)[36] should have evaporated from the sample. In addition, any orientation or mechanical stresses induced by the spin coating should have been annealed during the heating process.

3.1.3 Characterization Techniques

3.1.3.1 Differential Scanning Calorimetry

Samples of PMMA were heated in a vacuum oven at 120°C for 24 hours to drive off any moisture that had been absorbed. One sample of approximately 15 mg was placed in aluminum pans in a TA Instruments DSC 2920. The sample was equilibrated at 25°C and then heated from 25°C to 180°C at 10°C/min for the first run. The sample was then cooled slowly, again equilibrated at 25°C and the heating process was repeated for a second run. All of these tests used nitrogen as a purge gas. The glass transition function in TA Instrumental Analysis was used to calculate the T_g of the material by finding the inflection point in the T_g step.

3.1.3.2 Gel Permeation Chromatography

A 3.160 mg/mL solution of PMMA in chloroform was prepared. One sample of 100 μL was injected into a Waters 150CALC GPC with an internal viscometer, Viscotek Model T60A, and an external refractive index instrument. The flow rate of the run was 1.000 mL/min.

3.1.3.3 Ellipsometry

A Woollam VB-200 Angle Spectroscopic Ellipsometer was used to acquire an accurate measure of film thickness. Wavelength scans were performed at 10 nm intervals from 350 to 1000 nm for incidence angles of 65°, 70°, and 75° for one sample of each film thickness. The curves were produced and fitted to model spectra. These stored plots contained three layers, a base of silicon, an oxide layer, and PMMA. The refractive index assumed for PMMA[7] was 1.492 leaving film thickness as the only variable to fit.

3.1.3.4 Dielectric Analysis

The spin coated samples were sputter coated with gold on top of the polymer to produce an electrically conductive surface. Two samples of each thickness were placed into a TA Instruments DEA 2970 Dielectric Analyzer and equilibrated at 35°C. The temperature was then ramped from 35°C to 150°C or 180°C at 2°C/min. The frequency sweep included 50,000, 60,000, 70,000, 80,000, 85,000, 90,000, 95,000, 100,000 Hz. A schematic of the instrument appears in Figure 3.1-1.

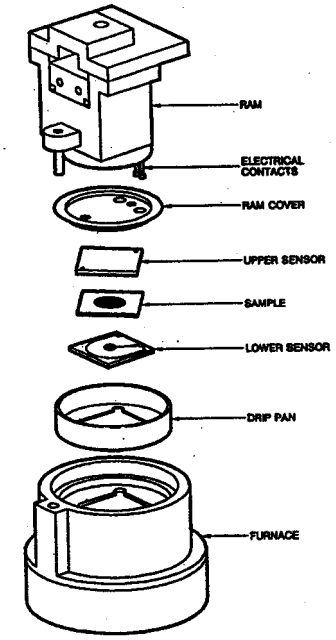

Figure 3.1-1: Schematic of Dielectric Instrument[37]

3.1.3.5 Thermal Mechanical Analysis

A TA Instruments DMA 2980 was used in penetration mode to measure the T_g of the PMMA films cast on silicon. Each sample was placed into a controlled temperature chamber, and a constant force of either 0.5 N or 1.0 N was applied to the surface of the film. After the temperature equilibrated at 30°C, the sample was heated from 30°C to 180°C at 2°C/min. A drop in the position of the penetration prove was used to calculate the T_g of the film. Three samples of the 900nm polymer film and two samples each of 660nm, 200nm, and 50nm polymer films and clean silicon were analyzed.

3.2 Polymer Brush Studies

3.2.1 Material

A polystyrene/poly*t*-butyl methacrylate (PS/PtBMA) di-block copolymer was previously synthesized for the polymer brush studies.[38] The molecular weight of the copolymer is approximately 50,000 g/mol with the m:n ratio approximately 1:1. The chemical structure of the di-block copolymer appears in Figure 3.2-1.

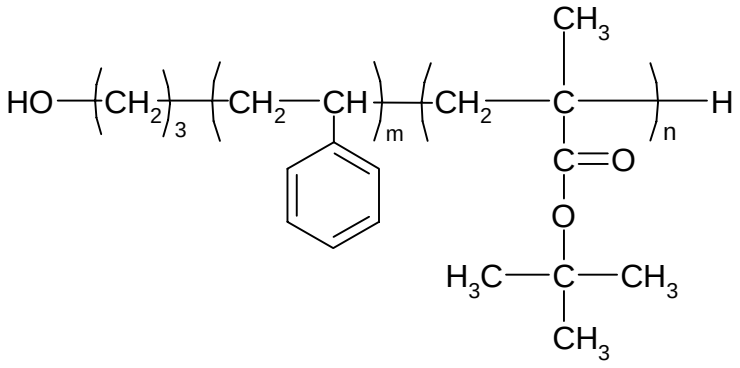

Figure 3.2-1: Chemical structure of di-block copolymer.

3.2.2 Sample Preparation

3.2.2.1 Surface Treatement

The silicon wafer surface was prepared in the same manner as that for the cooperativity studies (see section 3.1.2.1).

3.2.2.2 Spin Coating

A 1.0% solution by weight was prepared by dissolving 50 mg of copolymer in 5.0 mL toluene. A clean silicon wafer was set onto the spin coater and four drops of solution were placed on the surface. Each polymer brush sample was rotated at 1000 rpm for 1 minute.

3.2.2.3 Reaction Conditions

To chemically bond the polymer chains to the silicon surface the polymer brush samples required heat well above their T_g's. All samples were placed in a vacuum oven (25 Torr) at 170°C immediately following spin coating. The terminal OH groups reacted with the native oxide layer of the silicon wafer as demonstrated in literature.[39] The reaction time was varied by removing samples from the high temperature environment at 10, 20, 40, 100, and 200 hours. (Because the 200 hour sample results duplicated the 100 hour sample results, only results for the 100 hour sample are presented.) To remove any unreacted polymer, the samples were immersed in toluene and placed in a sonicator for a total of 34 hours at approximately 40°C.

3.2.2.4 Washing Procedure

After the unreacted polymer was removed, the films were washed with toluene and chloroform to alter the chain comformations. Analysis was performed to observe

polymer brush behavior after exposure to different solvents. The polymer brush samples were submerged in approximately 30 mL of the solvent at room temperature. After 10 minutes, the samples were removed and blown dry with a stream of air.

3.2.2.5 Hydrolysis

After the original polymer brush samples were characterized, hydrolysis was performed on the sonicated samples. The sample was submerged in a solution of 1 mL of concentrated HCl in 30mL of THF. After two hours, the sample was blown dry with a stream of air and washed in toluene. A fraction of the t-butyl side groups was hydrolyzed and replaced by polymethyl acrylic acid (PMAA) units, see Figure 3.2-2.

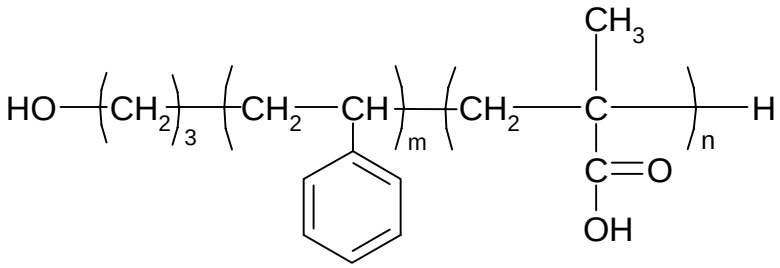

Figure 3.2-2: Chemical structure of di-block copolymer after hydrolysis.

3.2.2.6 Sample Nomenclature

Three major variables were investigated in this polymer brush study: the initial reaction time of the sample, the solvent last used to wash the sample, and the effect of a hydrolysis reaction. As the samples are discussed, the number depicts the reaction time, the next letter represents the solvent (t, toluene; c, chloroform), and a "h" indicates a hydrolyzed polymer. For example, 40ht means the sample has a reaction time of 40 hours, was last washed in toluene, and has been hydrolyzed. A complete listing of all the polymer brush samples prepared appears in Table 3.2-3.

Table 3.2-3: Polymer brush samples prepared.

Sample	Reaction Time	Wash Solvent	Hydrolyzed
10t	10 hours	toluene	
20t	20 hours	toluene	
40t	40 hours	toluene	
40ht	40 hours	toluene	x
100t	100 hours	toluene	
100c	100 hours	chloroform	
100ht	100 hours	toluene	x
100hc	100 hours	chloroform	x
200t	200 hours	toluene	

3.2.3 Characterization Techniques

3.2.3.1 Ellipsometry

The ellipsometry procedure was equivalent to that followed in the cooperativity studies (see section 3.1.3.3). The toluene washed and hydrolyzed samples were each analyzed once; the instrument averaged the properties across the entire width of the sample.

3.2.3.2 Contact Angle Analysis

An optical goniometer (DAGE 650) was used to measure contact angles. Static contact angles were measured with 3μL of both deionized water and methylene iodide (99% pure, Acros Organics). Measurements were taken on both sides of the drop and averaged to reduce error. The contact angles reported for each sample are the average of five measurements.

3.2.3.3 X-ray Photoelectron Spectroscopy

X-ray Photoelectron Spectroscopy (XPS) was performed using a PHI Perkin Elmer model 5400 spectrometer. Two samples were analyzed: 20t and 20ht. Atomic concentration tables were generated, and in addition, element analysis of oxygen and carbon was performed on both samples.

3.2.3.4 Atomic Force Microscopy

A Digital Instruments Scanning Probe Microscope was used in the tapping mode for all AFM measurements as seen schematically in Figure 3.2-3. A silicon nitride tip was driven with a ratio of 3.0V (RMS) to 1.8V (Set point). At least three height and phase images were generated on a 5.0 μm, 2.0 μm, or a 1.0 μm square scale for each sample listed in Table 3.2-3. In addition, the difference in elevation for two specifically selected points on each polymer brush sample were measured.

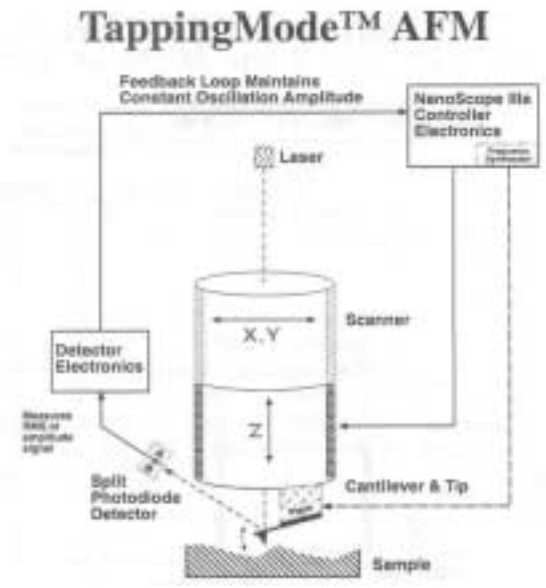

Figure 3.2-3: Schematic of AFM instrument.[40]

4 Chapter IV

Results and Discussion: Cooperativity Studies

4.1 Differential Scanning Calorimetry

Differential Scanning Calorimetry (DSC) was used to measure the T_g of PMMA. These measurements provided bulk values to compare to thin film properties. The sample was taken through a first heat, a slow cool (~ 1.3°C/min.), and a second heat. The DSC plots, heat flow versus temperature, endotherm up, appear in Figure 4.1-1 with the T_g shown as a step. The resulting T_g values were 103°C for the first heat and 104°C for the second heat. These values correlated well with the literature value of 104°C.[7]

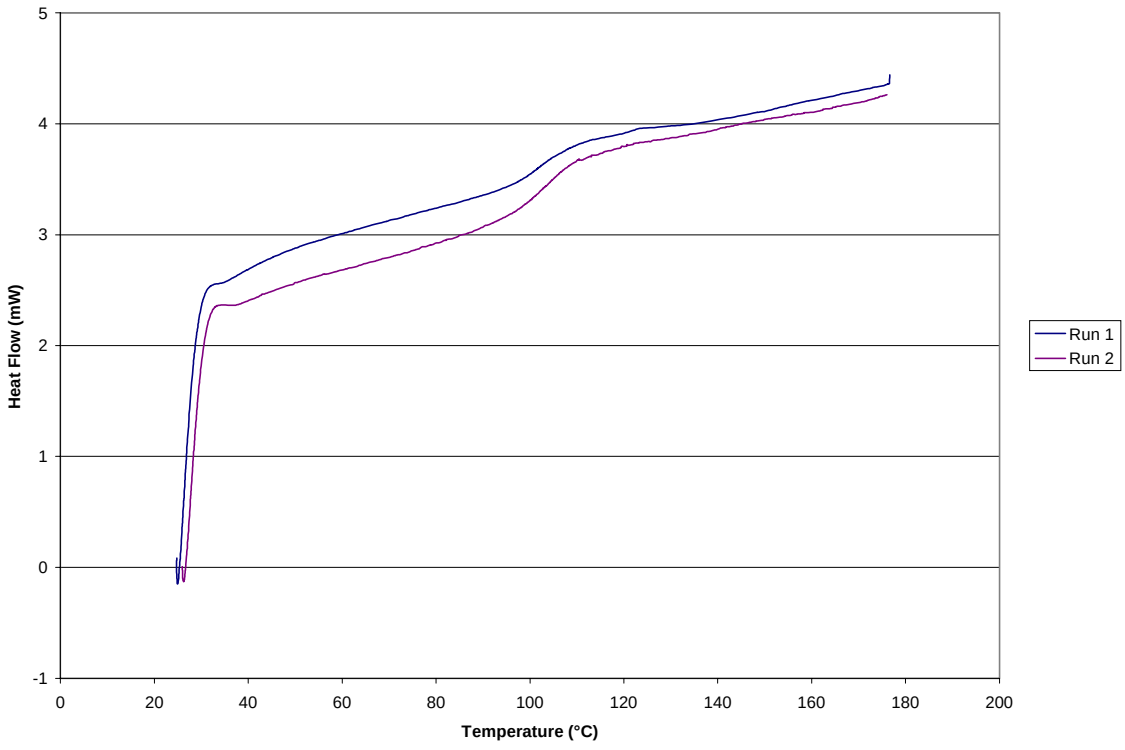

Figure 4.1-1: DSC scan of PMMA (Endotherm Up)

4.2 Gel Permeation Chromatography

Low molecular weight polymers have many chain ends and therefore have a high free volume; as a result, the polymer has very low dependence on the coupling parameter.[41] To assure a measurable difference in cooperativity, an accurate measure of the molecular weight of PMMA was needed. Gel Permeation Chromatography (GPC) results showed a weight average molecular weight of 101,300 g/mol and a number average molecular weight of 51,500 g/mol for the PMMA of this study. This relatively high molecular weight provided an excellent system to study. The polydispersity was 1.967 indicating a broad distribution of molecular weights. The chromatogram can be observed in Figure 4.2-1.

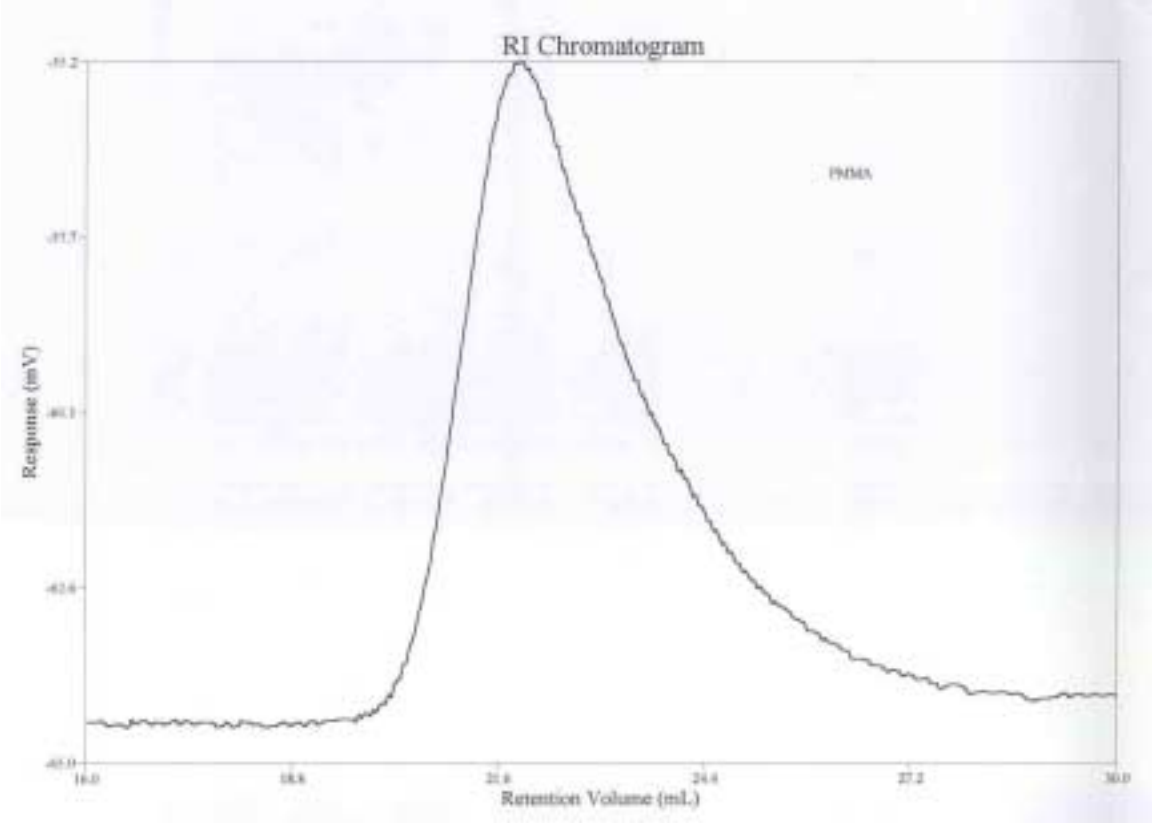

Figure 4.2-1: GPC results for PMMA

4.3 Ellipsometry

Ellipsometry provided accurate and reproducible measurement of film thickness to correlate with the cooperativity of the polymer. The film thickness for each of the polymer film systems prepared from 2%, 5%, and 10% solutions was recorded in Table 4.3-1, Table 4.3-2, and Table 4.3-3 respectively. Each row represents one sample giving a total of twenty samples. The error was determined by the difference in the experimental and model curves for each sample; overall, the error was a small percentage of the film thickness.

Table 4.3-1: Film Thickness and error for 2% PMMA solution

2% PMMA in Toluene		
Spin Speed (rpm)	**Thickness (nm)**	**Error (nm)**
3000	47.14	0.0713
3000	52.09	0.147
3000	52.14	0.083
3000	52.79	0.149
2000	73.07	0.132
1500	78.68	0.113

Table 4.3-2: Film Thickness and error for 5% PMMA solution

5% PMMA in Toluene		
Spin Speed (rpm)	**Thickness (nm)**	**Error (nm)**
3000	189.21	0.101
2500	209.69	0.151
1900	214.82	0.374
1900	218.16	0.372
1750	243.42	0.325
1500	272.90	0.351
1250	284.44	0.401

Table 4.3-3: Film Thickness and error for 10% PMMA solution

10% PMMA in Toluene		
Spin Speed (rpm)	**Thickness (nm)**	**Error (nm)**
3000	659.42	1.94
2500	661.87	1.91
1250	898.00	4.50
1250	898.00	3.50
1250	900.00	3.29
1250	900.00	3.59
1250	900.00	3.32

A bar graph was constructed to illustrate the range of film thickness produced. As noted in Figure 4.3-1, films from 50 nm to 900 nm were made. The research planned to analyze a series of polymer films from 100 to 500 nm were. The 900 nm series of 10% solutions provided evidence for the precision of the spin coater. All five samples were within 2.0 nm of each other in film thickness. Similar checks for repeatability were made by preparing two samples consecutively and identically (for 215 nm and 50 nm).

Solution concentrations did have a large effect on the film thickness. The effect can be seen in the large jump between a 284 nm maximum for the 5% solution and a 659 nm minimum for the 10%. Also, the film thickness vs. solution concentration was plotted for the 3000 rpm spin speed to demonstrate this dependence (Figure 4.3-2). In total, spin coating and ellipsometry together provided repeatable samples and accurate measurements of film thickness.

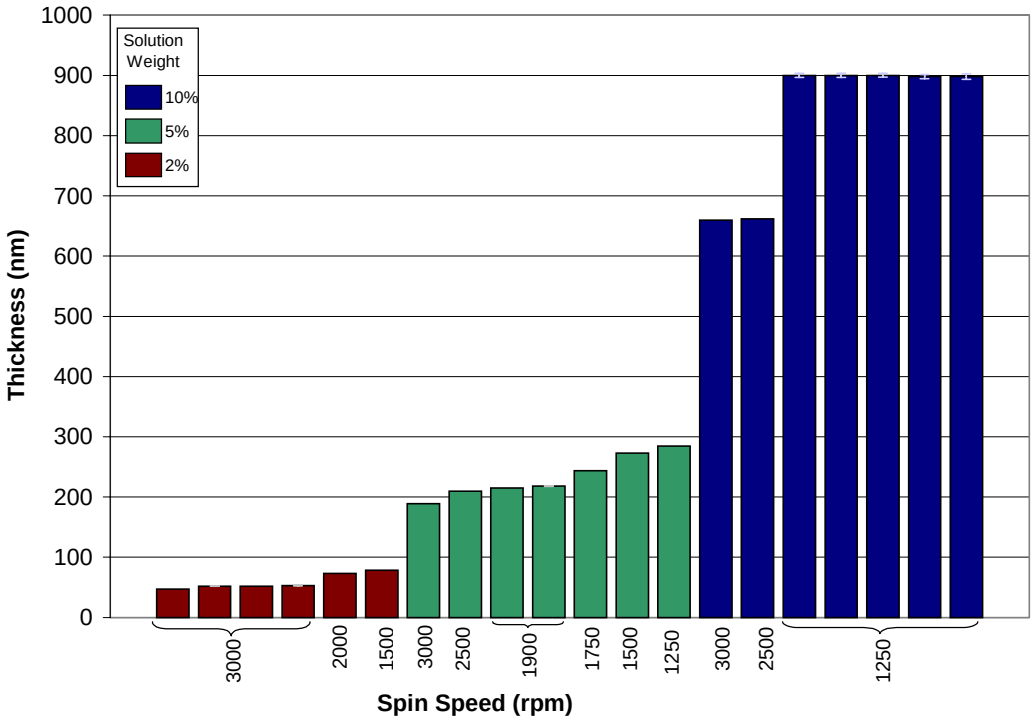

Figure 4.3-1: Film Thickness versus Spin Speed for each sample

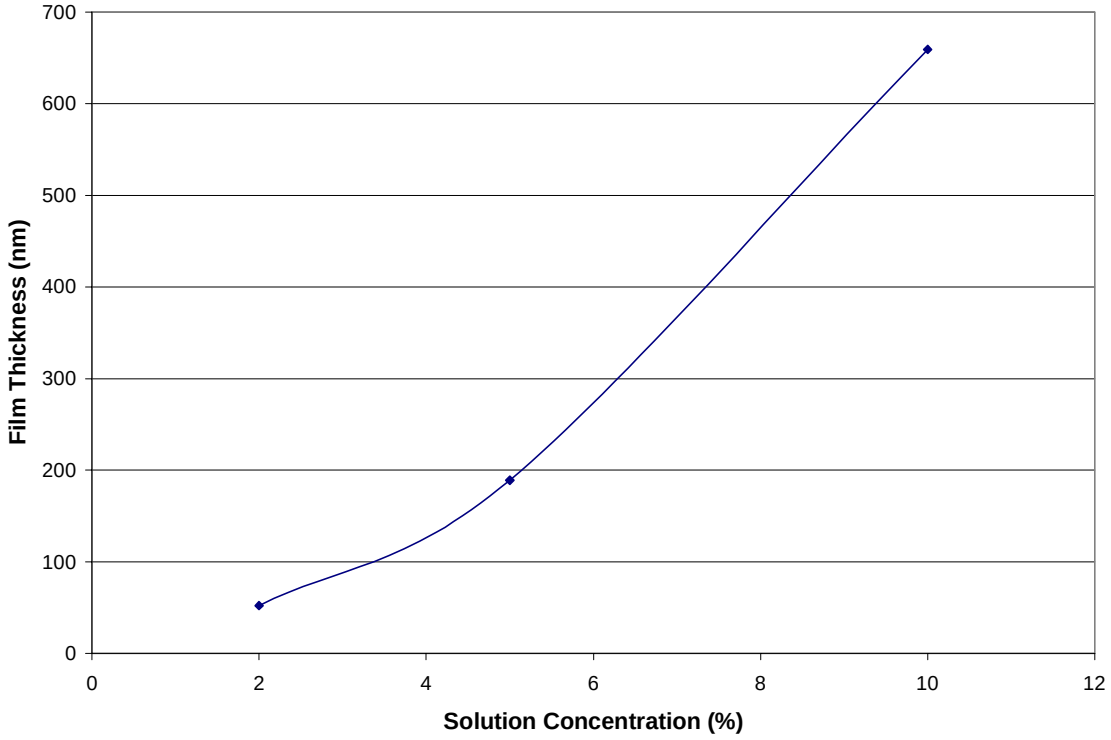

Figure 4.3-2: Film thickness vs. solution concentration for the 3000 rpm samples

4.4 Dielectric Analysis

Dielectric analysis (DEA) using both temperature and frequency sweeps can provide a direct measure of cooperativity. Because silicon is a semi-conductor, there were some concerns about consistent permittivity. The current would have to be high enough to allow the silicon wafer to conduct. The first test, then, was on a clean silicon wafer.

Before a run was begun, the permittivity was checked to test for the ability to measure silicon. The literature value, 4.0,[42] was used for comparison. When a reasonable and stable value for permittivity was reached, the run was begun. Figure 4.4-1 shows the permittivity of the silicon over the range of temperatures used. Although the value of permittivity began at a reasonable value, it increased as the temperature increased. This increase could have been caused by a build up of charge between the plates.

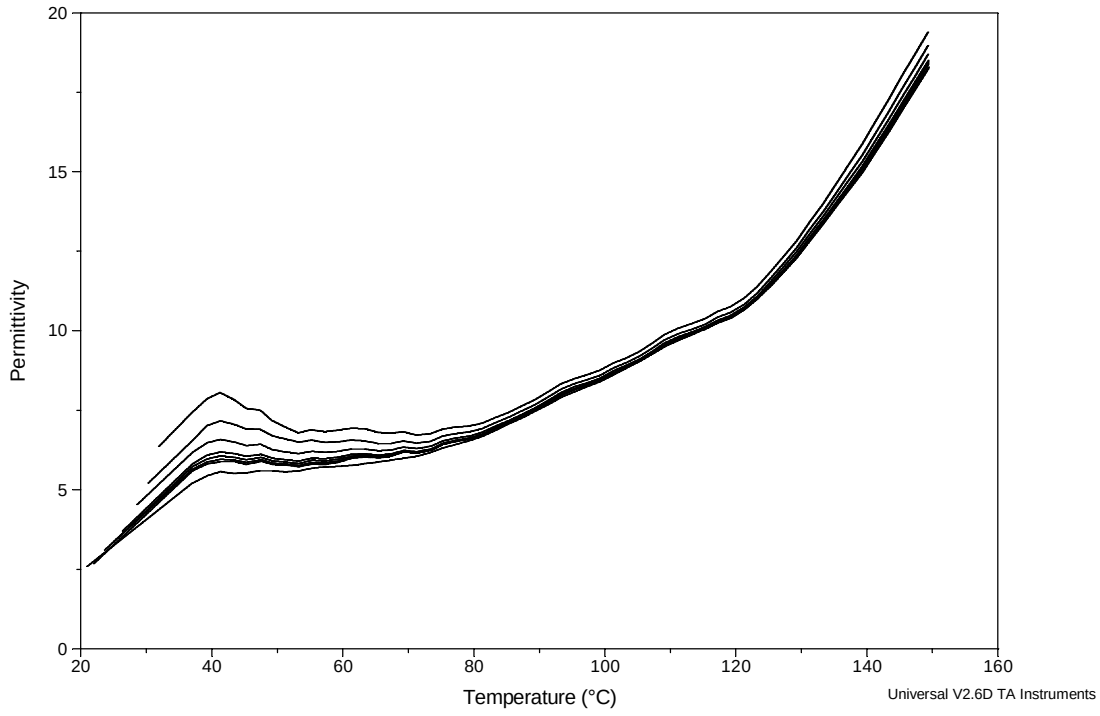

Figure 4.4-1: DEA results for clean silicon wafer, permittivity as temperature increased

The parameter of concern for the polymer measurements was the dielectric tan delta, defined as the dielectric loss modulus divided by the dielectric permittivity. To create a baseline for the system, a clean silicon wafer was analyzed; the tan delta values were reported in Figure 4.4-2.

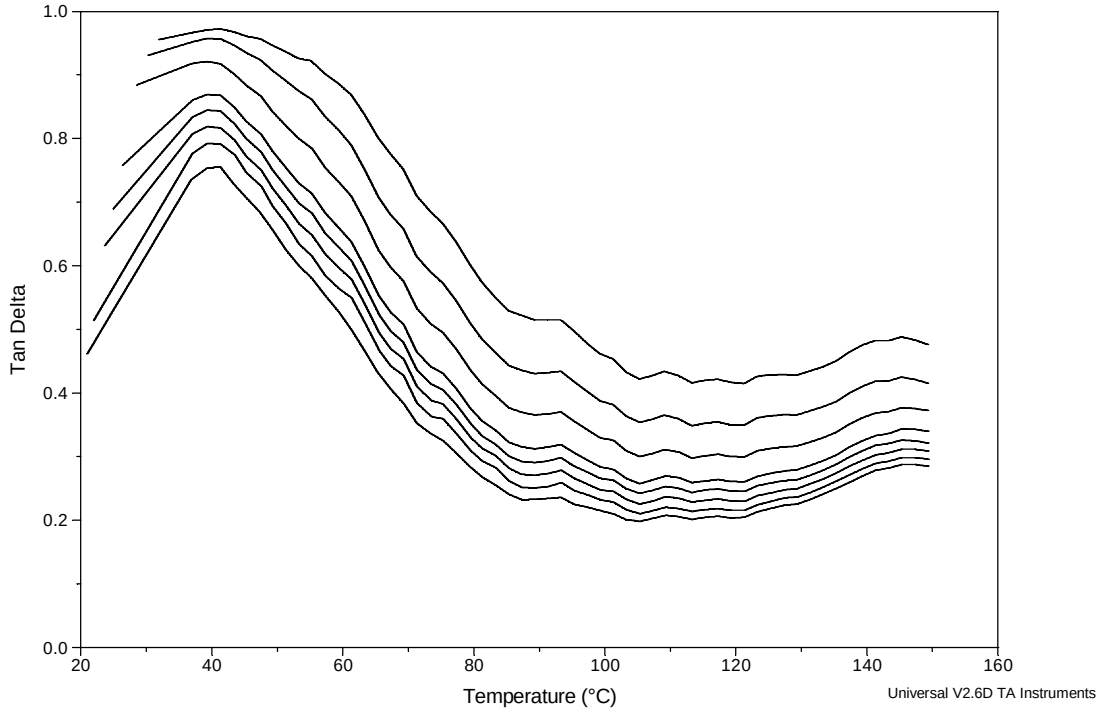

Figure 4.4-2: DEA of clean silicon wafer

To observe how a thin film would perform in DEA, several runs of the polymer films on silicon were done. An example of the tan delta values for one 50 nm film can be seen in Figure 4.4-3. The plot closely resembled those of the blank silicon wafers. The instrument appeared not to have the sensitivity to measure these thin films. The transitions of the polymer seemed to be masked by the bulky silicon substrate. The thicker films of 200 nm and 900 nm never gave an accurate initial permittivity and, therefore, the temperature sweeps were not performed.

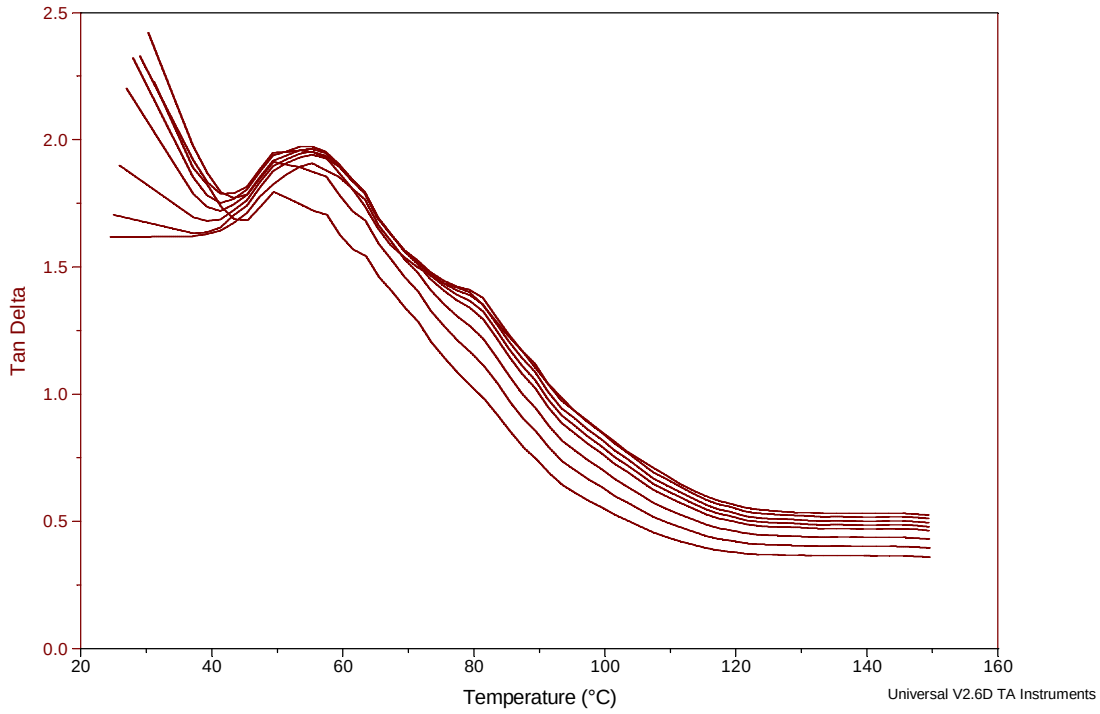

Figure 4.4-3: DEA results of 50 nm PMMA film on silicon

A second sample was tested for reproducibility and gave strikingly different results (Figure 4.4-4). A concern was raised over the repeatability of the measurement. A second sample of clean silicon was run and these results also looked dramatically different. (Figure 4.4-5). Due to insensitivity of the instrument and non-reproducible data, a direct measurement of the cooperativity of this system was not possible with dielectric analysis.

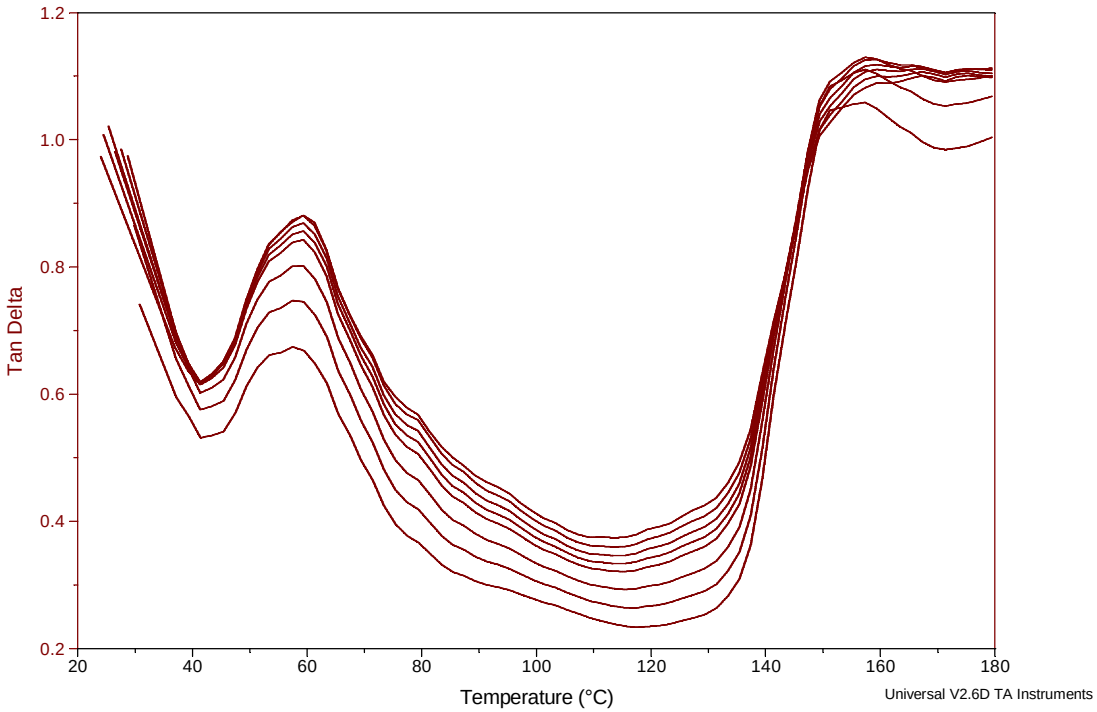

Figure 4.4-4: DEA results of a second 50 nm film sample on silicon

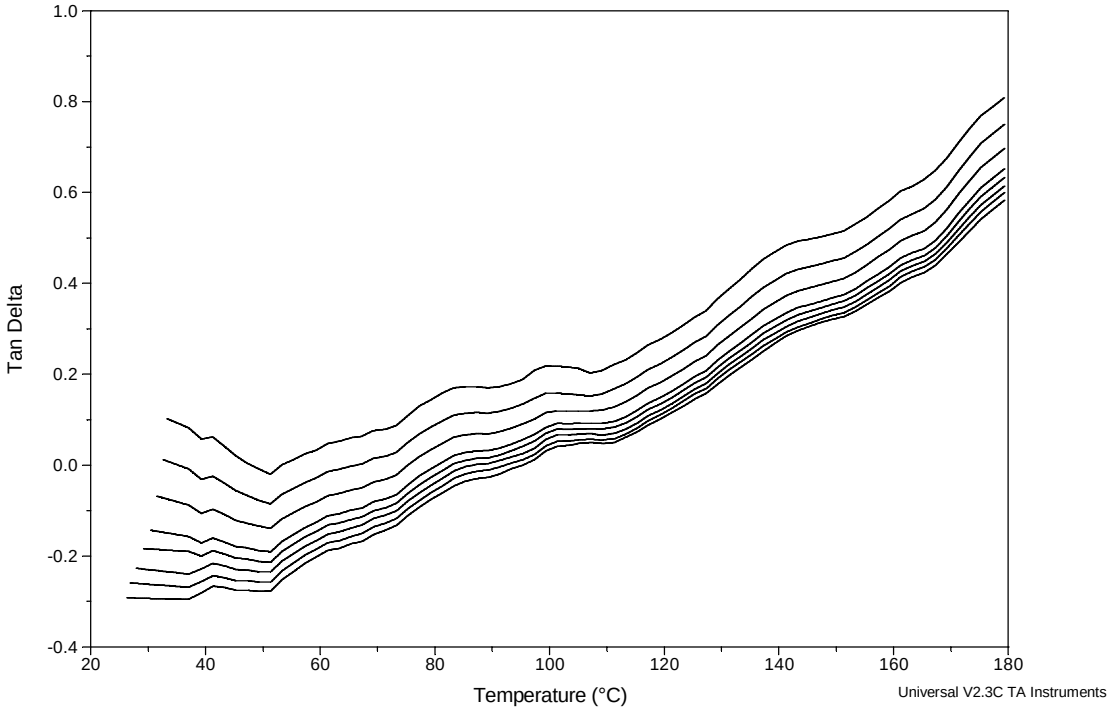

Figure 4.4-5: DEA results of a second clean silicon wafer sample

4.5 Thermal Mechanical Analysis

With a direct measurement of cooperativity of the thin films via dielectric spectroscopy not attainable, attention was turned to probing the system indirectly. As discussed previously, changes in the glass transition temperature can indicate changing cooperativity. Thermal mechanical analysis (TMA) was used to survey the T_g of the system. Due to the favorable interactions of the PMMA side chains and the native oxide layer of silicon, the thinner films were expected to increase in cooperativity and therefore show an increase in T_g. The tests were started with the thickest films, 900 nm.

As the system was heated, it expanded giving a constant increase in probe position. At the onset of the glass transition, the penetration probe should depress into the softening polymer. This depression appears to the instrument as if it observed a

decrease in dimension. The results for one 900 nm film can be seen in Figure 4.5-1. The T_g of this sample was 90 °C.

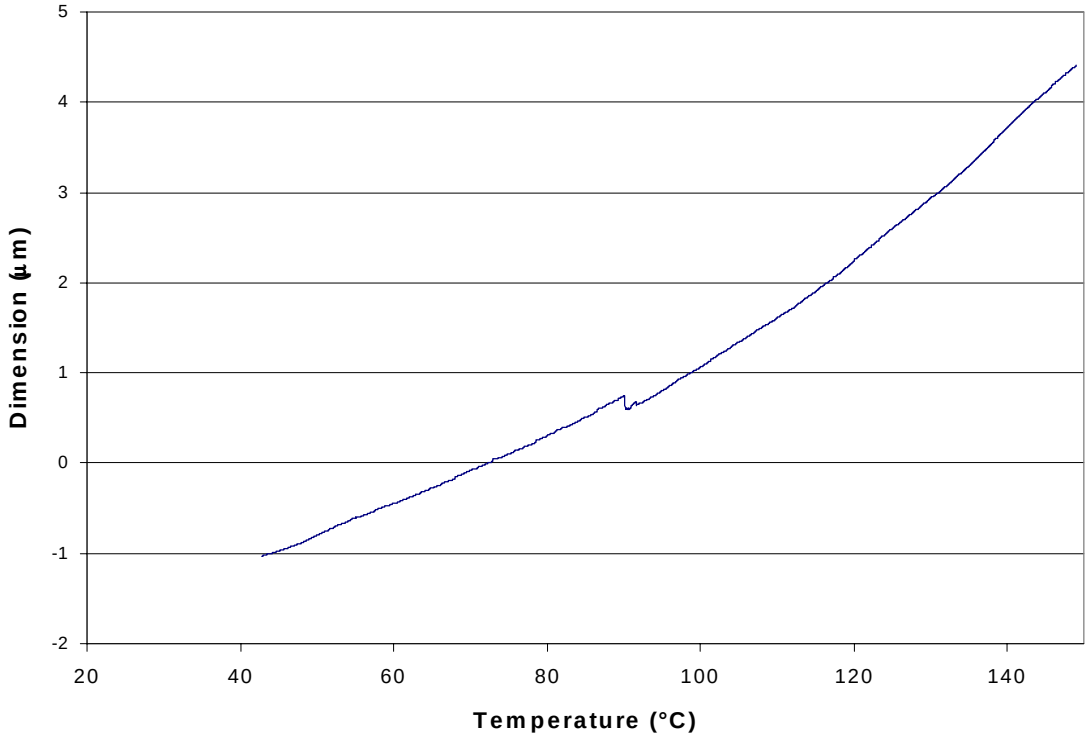

Figure 4.5-1: 900 nm DMA

The next step was to perform similar experiments with the thinner films. Initially, the 200 nm and 50 nm samples were tested; as can be seen in Figure 4.5-2, no decrease in probe position was observed. The instrument was believed to be not sensitive enough to detect these nanometer changes in position. Therefore, a thicker film of 660 nm was tested; again, no depression was seen. Figure 4.5-3 shows the 660 nm run superimposed on a run of a clean silicon wafer. The thermal expansion of PMMA and silicon ran parallel to each other after 60°C. Again, the bulky substrate seemed to overpower the properties of the thin film. TMA, then, seemed unable to accurately measure such a small change in dimension.

The instrument manual only presents a range for a displacement measurement of 25 mm. However, the dynamic deformation, which uses the same drive shaft, can gauge

changes as small as 0.5 μm.[43] The instrument, then, is confined to quantifying changes of 500 nm or more, which is too large for the thin films of this research.

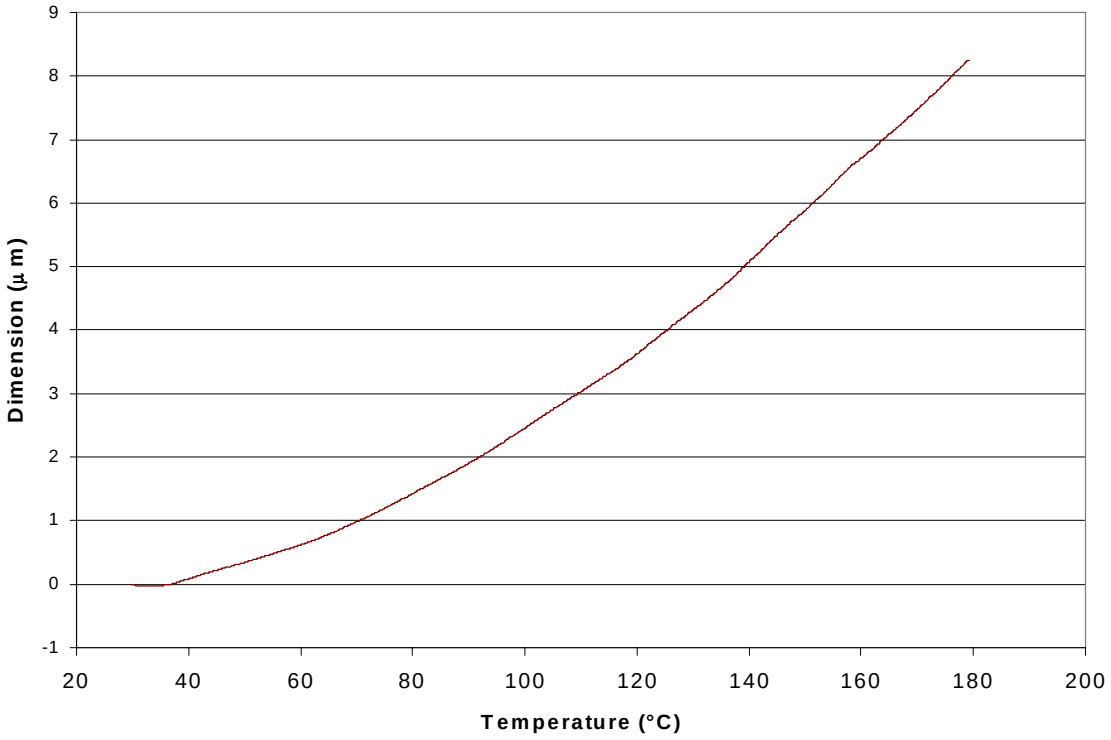

Figure 4.5-2: TMA results of 50 nm film of PMMA, no apparent transition

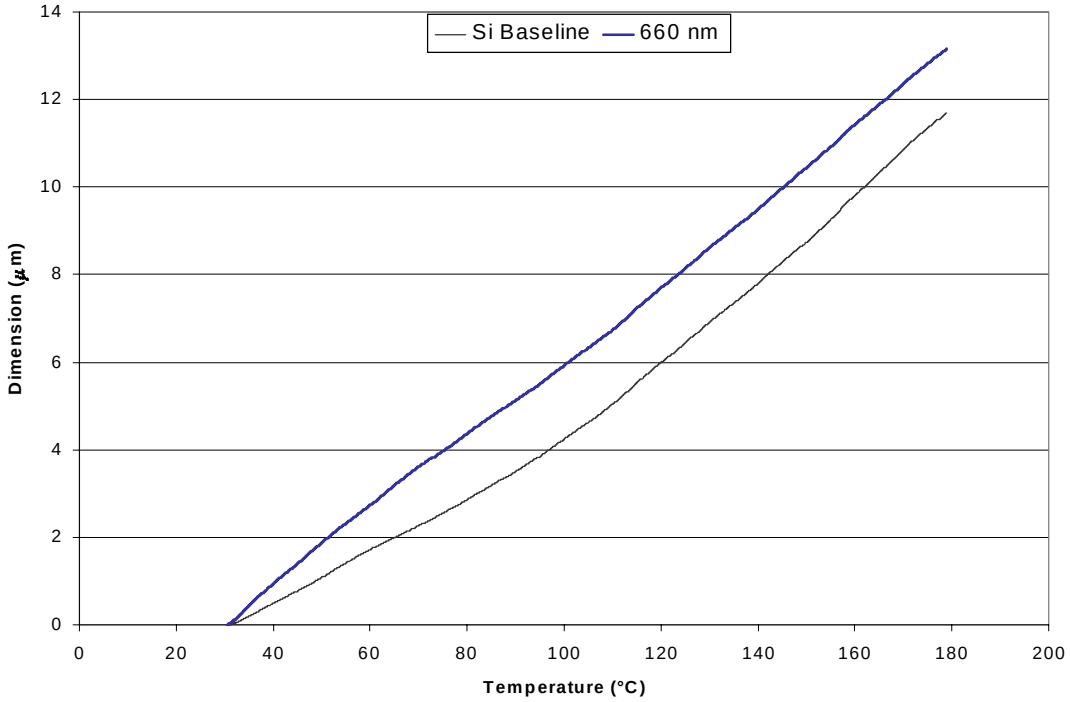

Figure 4.5-3: TMA results of 660 nm film superimposed on blank silicon wafer

4.6 Summary of Cooperativity Studies

The PMMA films were produced on silicon wafers, and the thickness was accurately measured by ellipsometry. Dielectric analysis was not a suitable technique for measuring the thermal transitions of a substrate and film system. Thermal mechanical analysis also proved to be insensitive to small changes in properties as a function of film thickness. Overall, the results of this study reinforced the difficulty of polymer characterization measurements on such thin supported films. On a positive note, this work verified the precision and reproducibility of preparing and measuring the thickness of such thin films using spin coating and ellipsometry. In future studies, instruments such as a heating stage coupled with an ellipsometer or a micro-thermal analyzer would be recommended. Once a method of reliable characterization is discovered, future work should include altering the surface chemistry and monitoring thin film behavior.

5 Chapter V

Results and Discussion: Polymer Brush Studies

5.1 Contact Angles

5.1.1 Contact Angle of Water

Contact angles were used to detect macroscopic changes in the surface chemistry of the samples. First, the contact angle of water was measured as a control on a clean (as defined in experimental section) silicon substrate and was 36.0°. The contact angle of water was determined for the polymer brush samples 20t, 40t, and 100t (reaction times of 20, 40, and 100 hours respectively, all washed in toluene, see Table 3.2-3); the contact angles were 79.3°, 89.8°, and 103.7°, respectively. An increase in the contact angle of water can be seen with an increase in reaction time. This increase in contact angle could be due to an increased grafting density and therefore greater polymer brush coverage.

The effect of the washing solvent was also investigated. The contact angles of water for samples washed in toluene and chloroform were compared. The 100c sample had a contact angle of 91.2°. The surface washed in chloroform was more polar compared that washed in toluene as illustrated by the 12.6° decrease in the contact angle of water.

The change in chemistry as the t-butyl group was replaced by hydrogen during hydrolysis should result in a decrease in the contact angle of water. As expected, the more polar, hydrolyzed sample showed such a decrease. For the 40ht sample the contact angle decreased by 10.1° from that measured for the 40t sample. The 100ht and 100t samples differed by 28.6°. Additionally, the 100hc sample demonstrated a 11.6° drop when compared to the 100c sample. These large decreases in the contact angles are evidence of successful hydrolysis.

A summary of the water contact angles can be seen in Figure 5.1-1; the error bars represent one standard deviation.

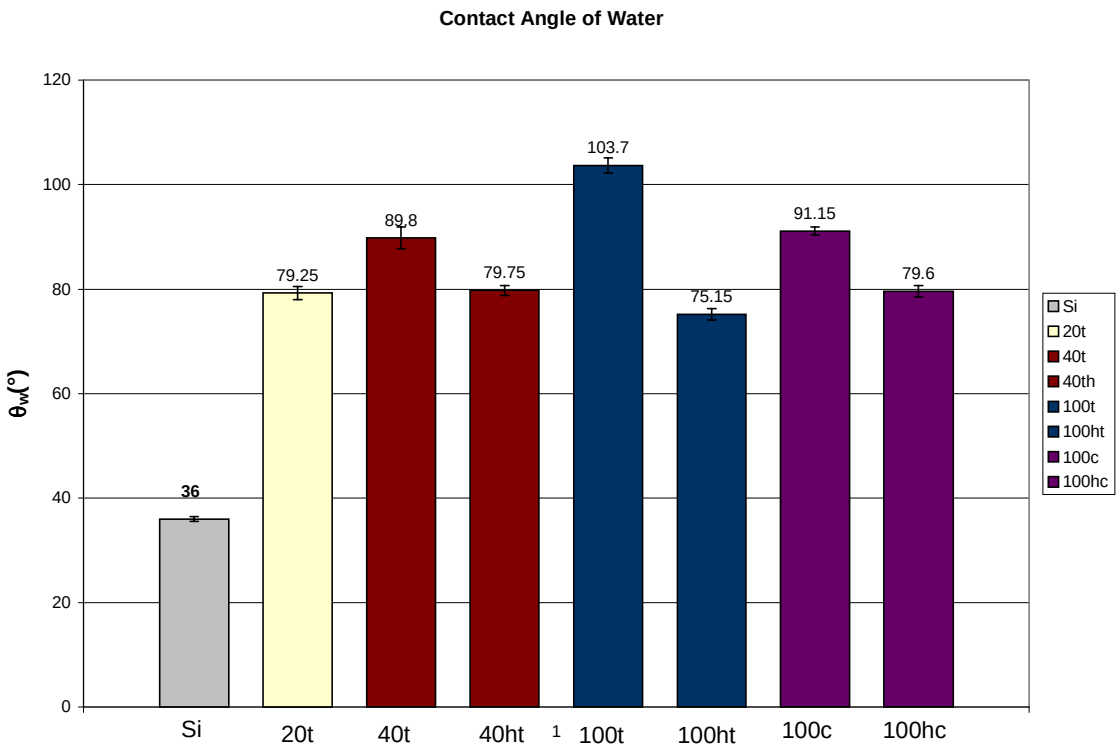

Figure 5.1-1: Contact angles of water on copolymer brush samples.

5.1.2 Surface Energy

The contact angle of methylene iodide was measured so that a surface energy for each sample could be calculated using a form of Young's equation (see section 2.8.1). The results appear in Table 5.1-1. The surface energy for the clean silicon substrate used as a control was 62.68 dyne/cm. The surface energy for all other samples fell in the range of 41-46 dyne/cm which corresponds well to the literature value of 42.6 dyne/cm for PS [31] but differs from the published value of 18.1 dyne/cm for P*t*BMA.[32] The reasons for this difference are unclear. The polar components of the surface energy (γ^p) increased as expected upon sample hydrolysis for both the 40 hour and 100 hour samples. A summary of this data can be seen in Table 5.1-2.

Table 5.1-1: Contact angles for methylene iodide.

Sample	θ_m (°)	Error (±°)
silicon	37.4	0.9
40t	31.4	1.4
40ht	34.3	1.1
100t	36.4	1.6
100c	35.8	0.7
100ht	33.2	1.3
100hc	29.5	3.1

Table 5.1-2: Surface energy with dispersive and polar components.

Sample	γ^d (dyne/cm)	γ^p (dyne/cm)	γ (dyne/cm)
silicon	28.1	34.5	62.7
40t	39.6	4.4	44.1
40ht	34.2	9.5	43.7
100t	40.3	2.6	42.9
100c	36.9	4.4	41.3
100ht	33.6	11.7	45.3
100hc	36.2	9.2	45.4

5.2 X-ray Photoelectron Spectroscopy

The polymer chains were bonded to the surface with a weak Si-O-Si-C bond. In acidic conditions there was a risk of cleaving the Si-O bond during hydrolysis. XPS was performed on one hydrolyzed sample to verify the presence of polymer on the surface. The results indicated a significant amount of carbon and oxygen on the surface (Table 3.2-1). The 15° take-off angle scan probed a depth of approximately 15 Å, and the 90° scan approximately 50 Å. Therefore, the 90° take-off angle scan was expected to reveal slightly more silicon (Table 3.2-2).

Table 5.2-1: XPS results (15°), atomic concentration table for one measurement of 20ht sample.

Element	Atomic Concentration (%)
C 1s	57.0
N 1s	1.2
O 1s	27.3
Si 2p	14.5
F 1s	< 0.1
Cl 2p	< 0.1

Table 5.2-2: XPS results (90°), atomic concentration table for one measurement of 20ht sample.

Element	Atomic Concentration (%)
C 1s	29.8
N 1s	0.9
O 1s	29.5
Si 2p	39.8
F 1s	< 0.1
Cl 2p	< 0.1

These XPS results can be compared to those of the polymer brush before hydrolysis (Table 5.2-3 and 5.2-4). The increase in the atomic concentration of oxygen for the hydrolyzed samples provides evidence of a successful hydrolysis reaction. In addition, analysis was performed on each of the oxygen peaks to determine the percent conversion for the hydrolysis; the oxygen peaks for the polymer side groups were not able to be resolved due to the presence of the dominant peak from the oxygen-silicon bond (Figures 5.2-1 and 5.2-2). Similarly, elemental analysis was performed on carbon and no quantitative analysis could be extracted from the resolvable peaks (Figures 5.2-3 and 5.2-4).

Table 5.2-3: XPS results (15°), atomic concentration table for one measurement of 20t sample.

Element	Atomic Concentration (%)
C 1s	90.9
N 1s	0.3
O 1s	7.6
Si 2p	1.2
F 1s	< 0.1
Cl 2p	< 0.1

Table 5.2-4: XPS results (90°), atomic concentration table for one measurement of 20t sample.

Element	Atomic Concentration (%)
C 1s	79.9
N 1s	0.3
O 1s	11.7
Si 2p	8.2
F 1s	< 0.1
Cl 2p	< 0.1

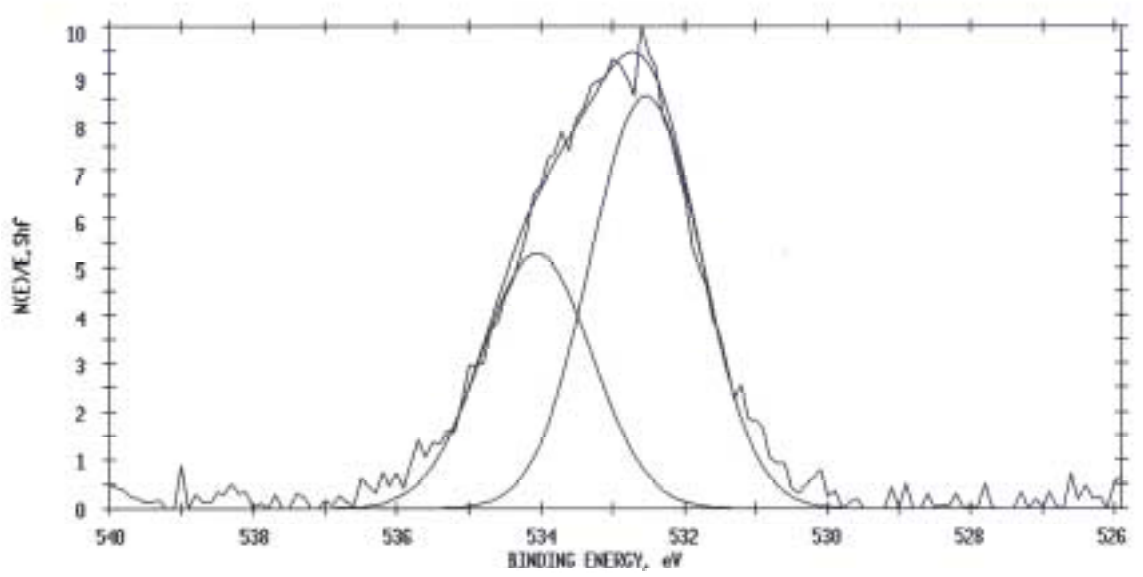

Figure 5.2-1: XPS elemental analysis of oxygen on 20t sample

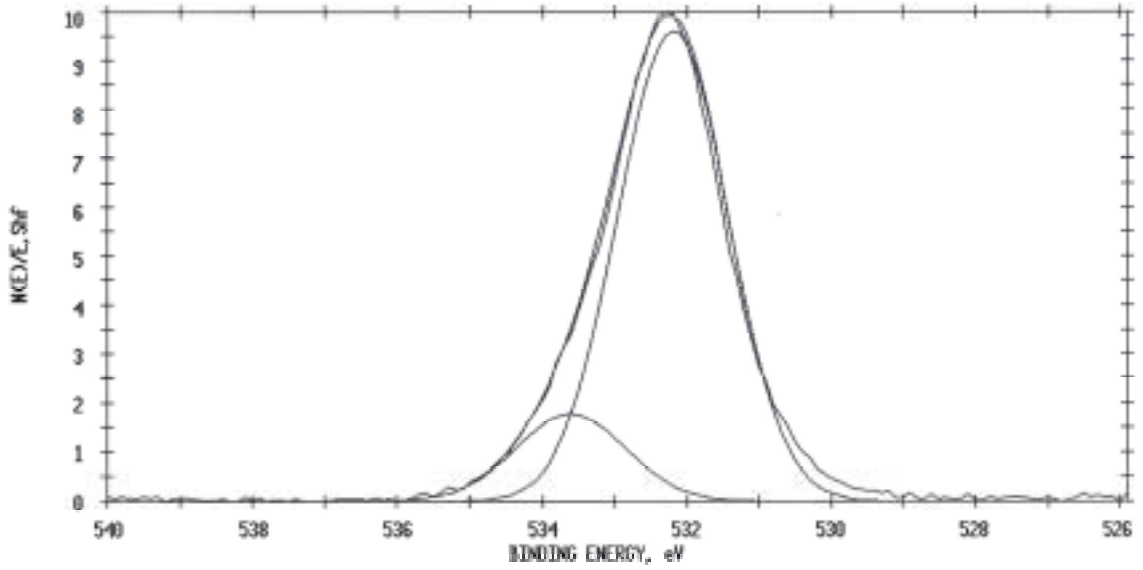

Figure 5.2-2: XPS elemental analysis of oxygen on 20ht sample

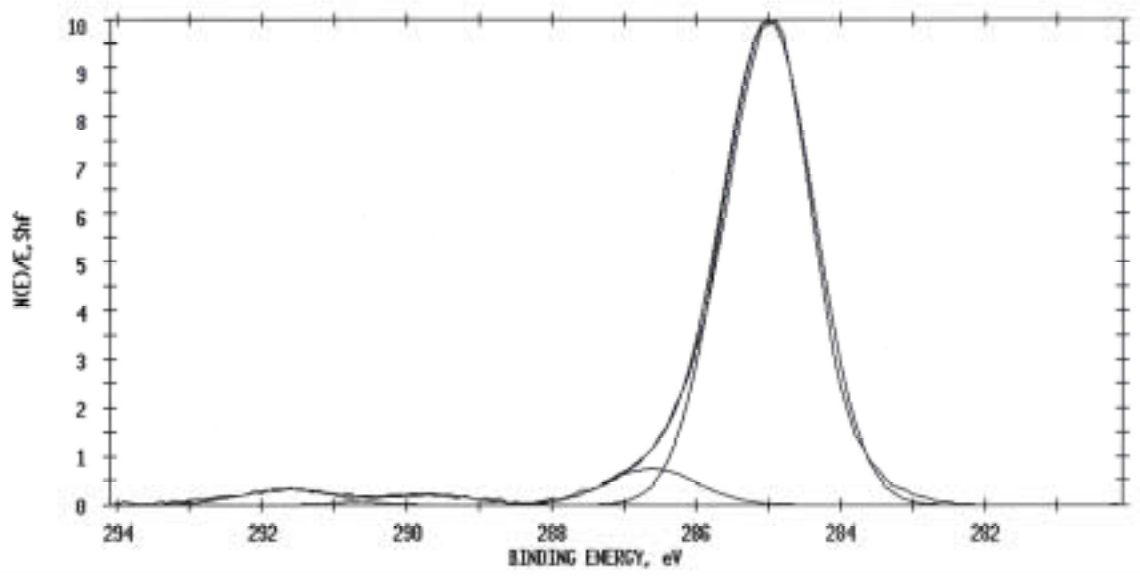

Figure 5.2-3: XPS elemental analysis of carbon on 20t sample

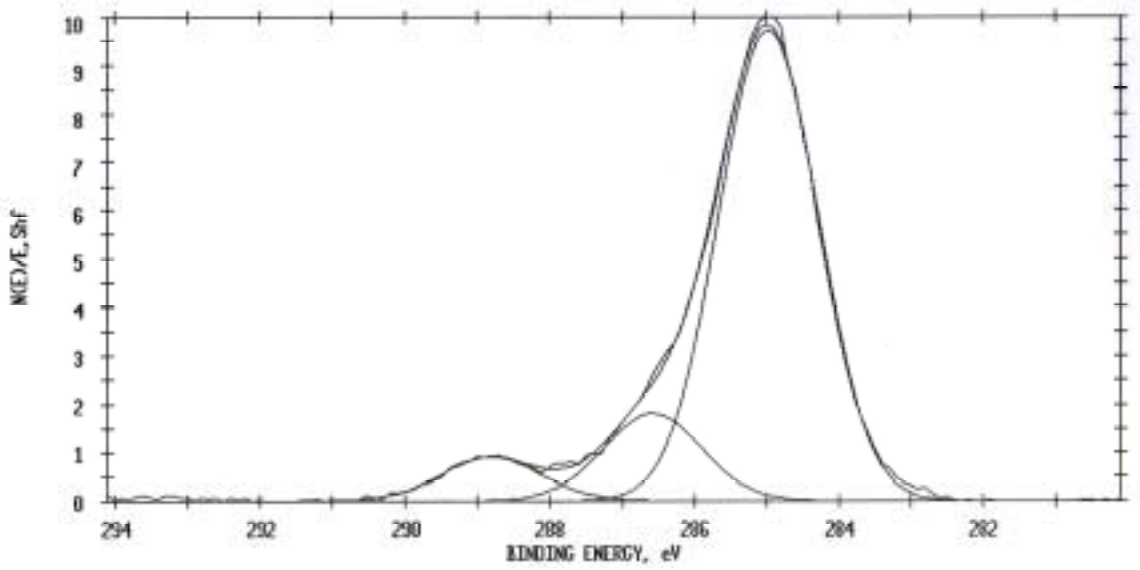

Figure 5.2-4: XPS elemental analysis of carbon on 20ht sample

5.3 Ellipsometry

Ellipsometry was used to measure the total thickness of the polymer brush plus absorbed layers. This value represented an average thickness over the whole polymer brush surface, not a specific point. Two trends were observed: an increase in film thickness with reaction time and a decrease in film thickness after hydrolysis.

Ellipsometry measurements were made after 10 hours of sonicating in toluene (Table 5.3-1) and again after an additional 24 hours of washing in toluene (Table 5.3-2). Initially a monolayer of polymer chains attached to the surface was expected. The thickness of such a polymer brush should be approximately 36.5 nm, the radius of gyration for the PS/P*t*BMA copolymer. Because the 40 and 100 hour samples were much thicker than this expected value, a lamellar layering of the copolymer is suspected. Such behavior has been reported in the literature (Figure 2.7-4).

As discussed in section 2.7, film thickness is dependent on grafting density. Ellipsometry results demonstrated a relationship between film thickness and reaction time (Tables 5.3-1, 5.3-2). It is suspected that these results demonstrate a relationship between reaction time and grafting density.

The film thicknesses of the hydrolyzed samples are listed in the last two rows of Table 5.3-2. In both cases, these results indicate thinner films for the hydrolyzed material samples. The acidic conditions seemed to have removed some of the existing layers, decreasing the overall thickness.

Table 5.3-1: Di-block sample film thickness from ellipsometry after 10 hours of washing

Sample	Thickness (nm)	Error (±nm)
10t	6.463	1.16
20t	13.44	0.378
40t	24.806	0.175
100t	48.106	0.528

Table 5.3-2: Di-block sample film thickness from ellipsometry after 34 hours of washing

Sample	Thickness (nm)	Error (±nm)
10t	8.1488	5.74
20t	14.424	0.182
40t	29.651	0.288
100t	39.129	0.291
40ht	17.193	2.08
100ht	7.9667	2.96

5.4 Atomic Force Microscopy

5.4.1 Height and Phase Images

Atomic force microscopy (AFM) was used to image the surface of each sample. All images presented are 2μm square in size. The height images show the relative heights of each point on the surface, with lighter colors corresponding to higher elevation. Similarly, the phase images show the relative moduli of each point on the surface, with lighter colors denoting softer regions. The data collected for the height image can be manipulated to generate a 3-dimensional (3-D) view of the polymer brush sample. The 3-D visualization aids in interpreting the height and phase images.

The first sample imaged was a clean silicon wafer (Figure 5.4-1 and 5.4-2). The sample is relatively flat with a roughness value of 5.21nm.

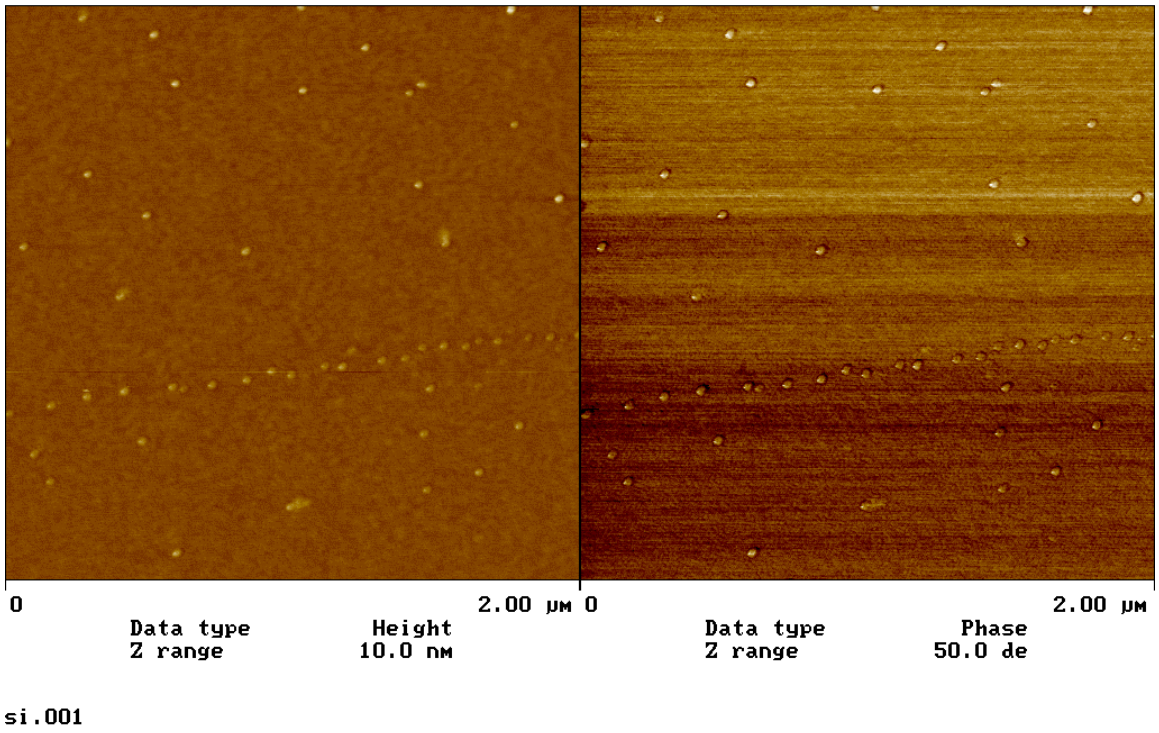

Figure 5.4-1: AFM image of a clean silicon wafer.

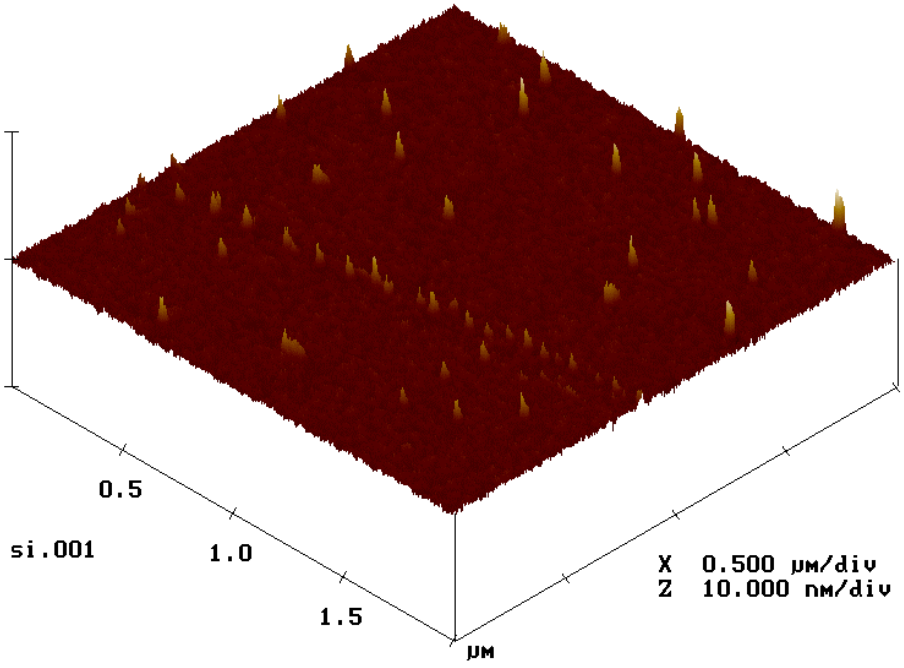

Figure 5.4-2: 3-D AFM image of a clean silicon wafer

AFM measurements were made after the polymer brush samples had been washed in toluene for 10 hours. The image of the 40t sample showed a worm-like structure on the surface of the polymer brush (Figure 5.4-3). This structure was more pronounced in the 100t image (Figure 5.4-4). Upon closer examination the image of the 40t sample indicated at least one additional layer of polymer below the worm-like structure (circled area in Figure 5.4-3). It is thought that this layer corresponded to the polymer brush, with the worm-like structure being caused by subsequent absorbed layers. This observation, coupled with the larger than expected film thicknesses (section 5.2), led to the conclusion that 10 hours of washing the samples had not removed all of the unreacted polymer from the surface.

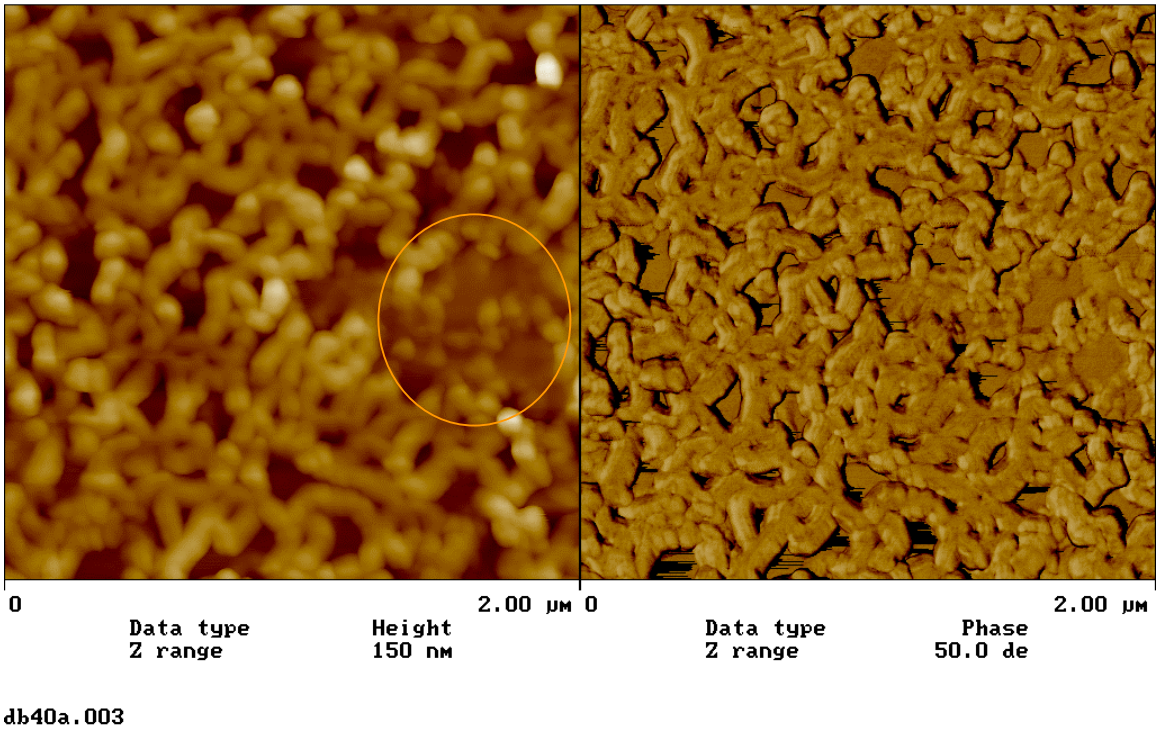

Figure 5.4-3: AFM image of 40t sample after 10 hours of toluene wash.

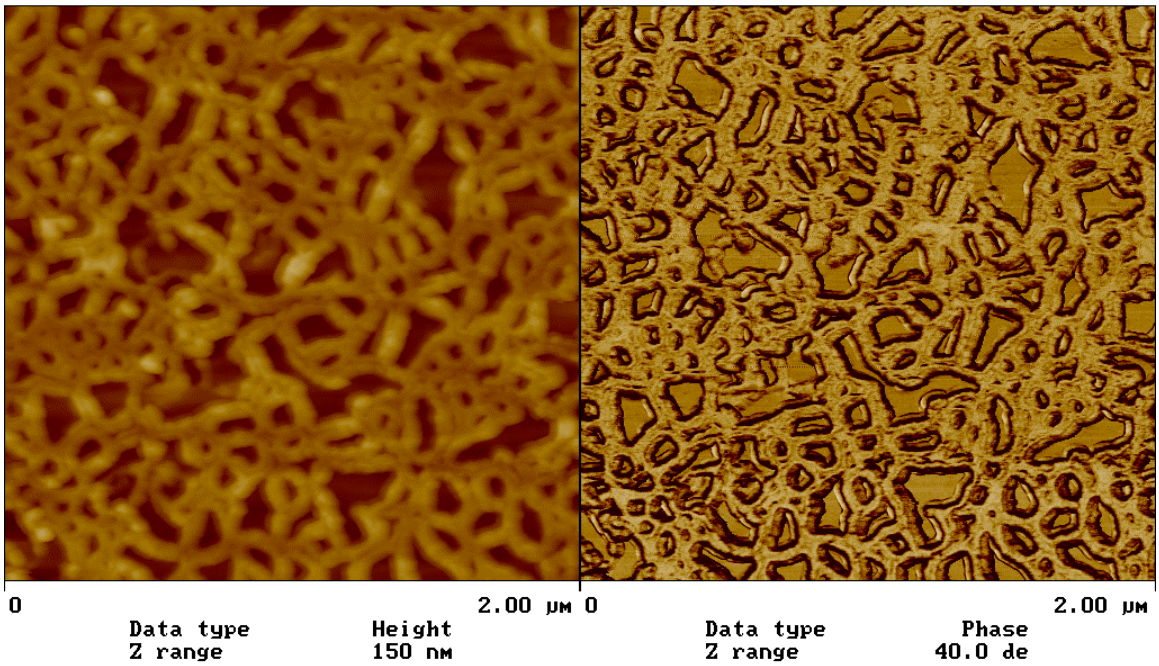

Figure 5.4-4: AFM image of 100t sample after 10 hours of toluene wash.

The polymer brush samples were washed in toluene for an additional 24 hours in an attempt to remove the absorbed layers from the surface. AFM images after the additional washing were taken of the 10t, 20t, 40t, and 100t samples. These polymer brush images were examined to look for qualitative trends in the morphology. In addition, measurements were made of the horizontal size of features on each surface. Qualitatively, there appeared to be an increase in the amount of morphological structure corresponding to an increase in the initial reaction time. Feature size also grew with the reaction time. The images can be viewed in Figures 5.4-5 through 5.4-12.

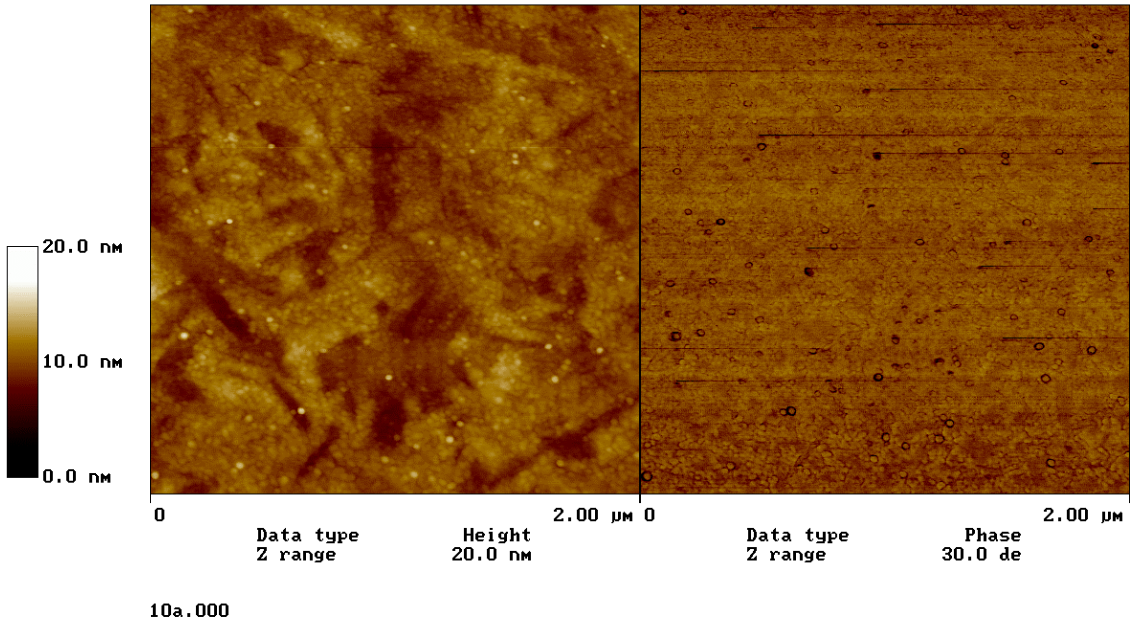

Figure 5.4-5: AFM images of 10t sample.

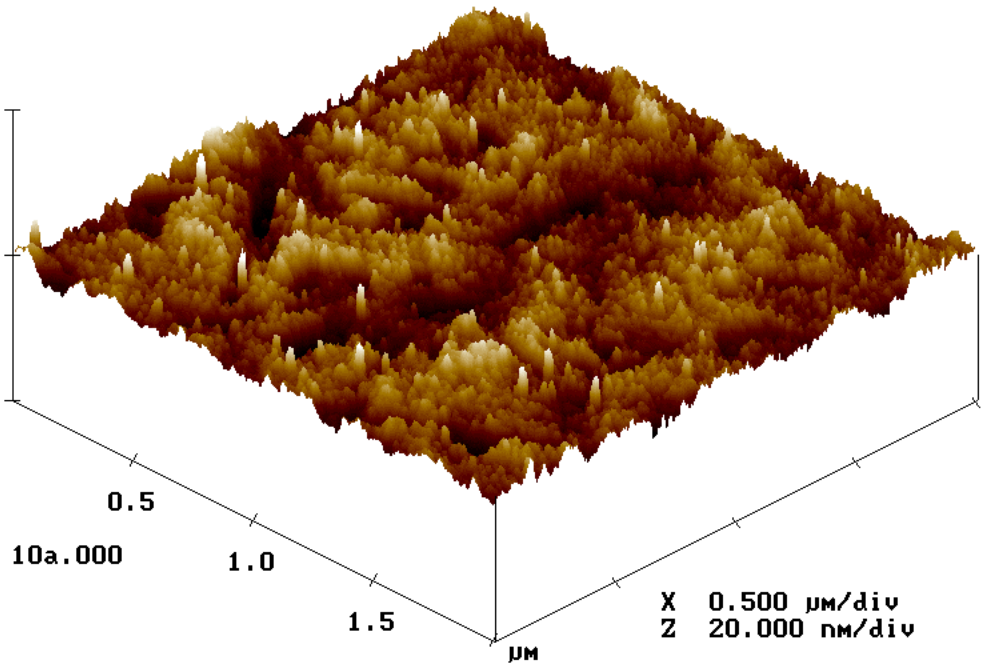

Figure 5.4-6: 3-D AFM image of 10t sample.

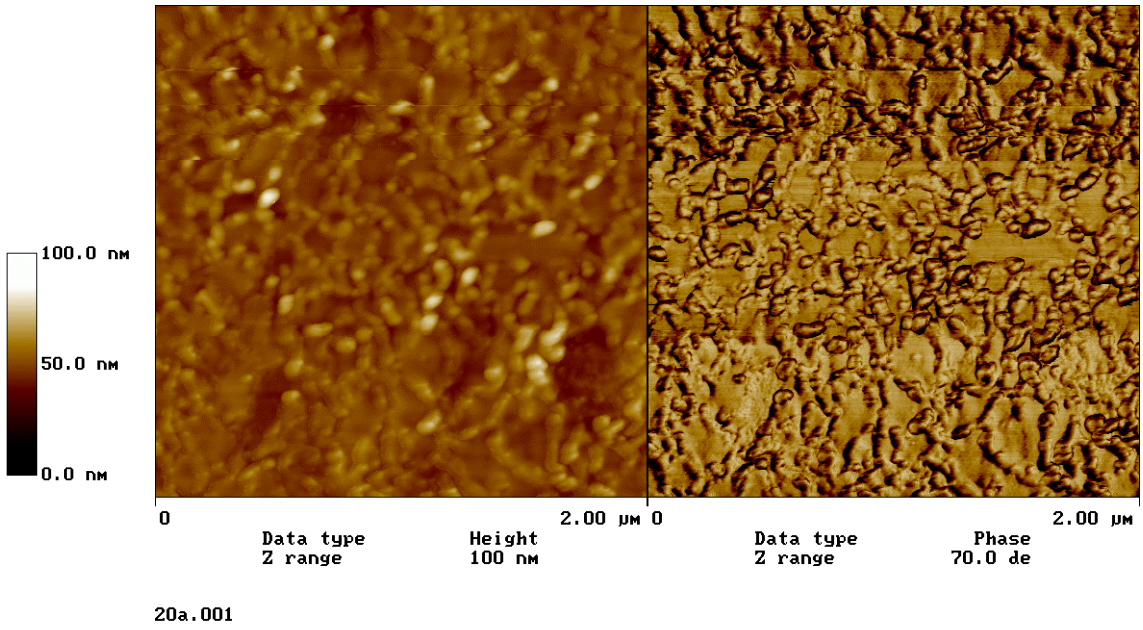

Figure 5.4-7: AFM images of 20t sample.

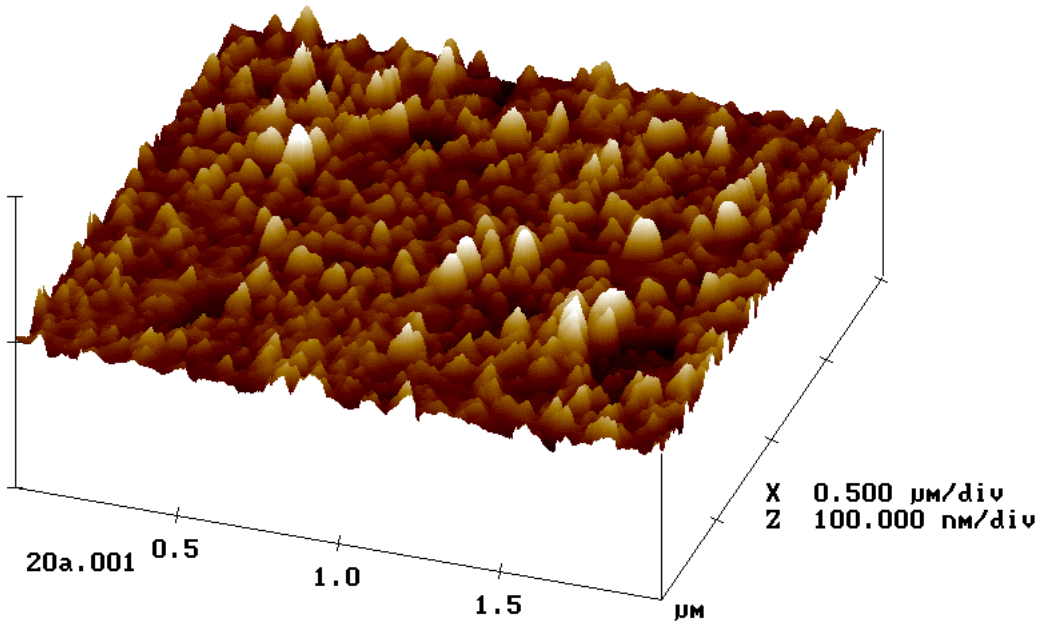

Figure 5.4-8: 3-D AFM image of 20t sample.

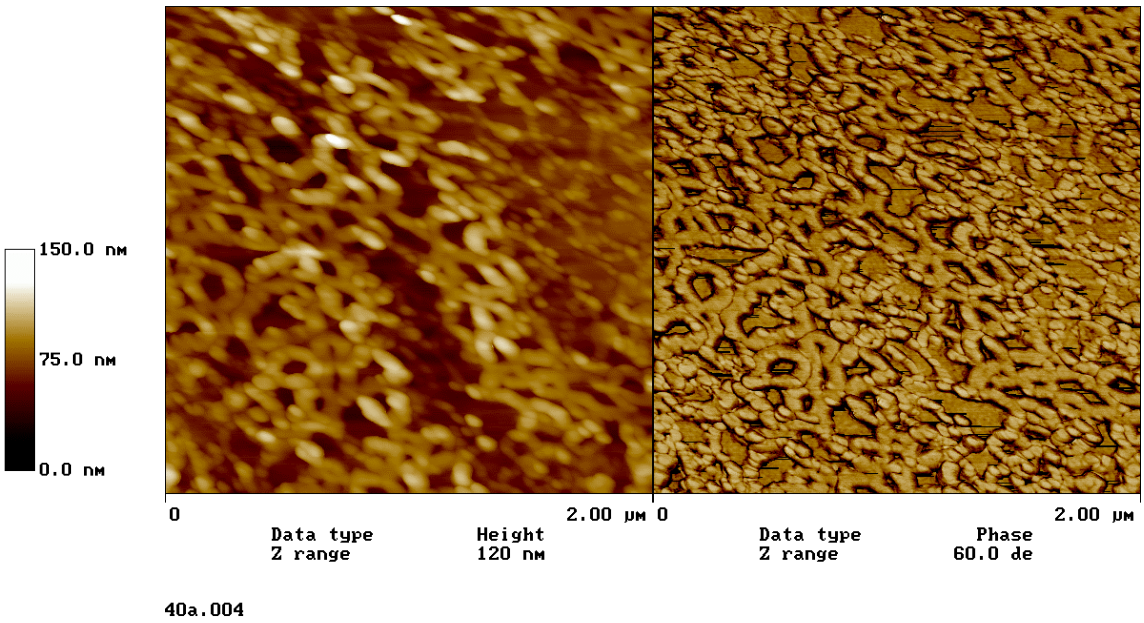

Figure 5.4-9: AFM images of 40t sample.

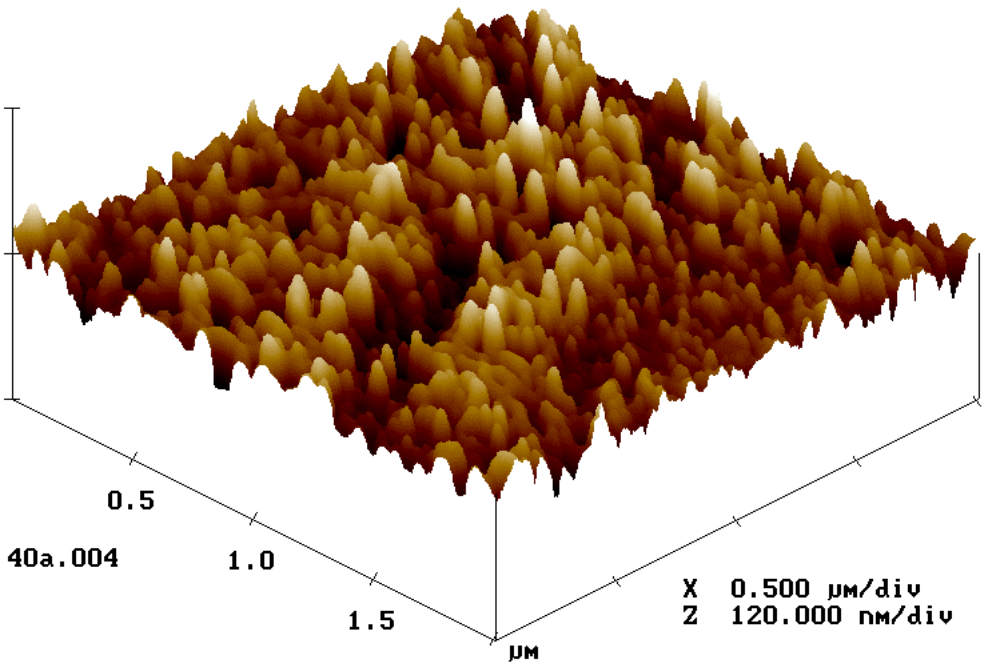

Figure 5.4-10: 3-D AFM image of 40t sample.

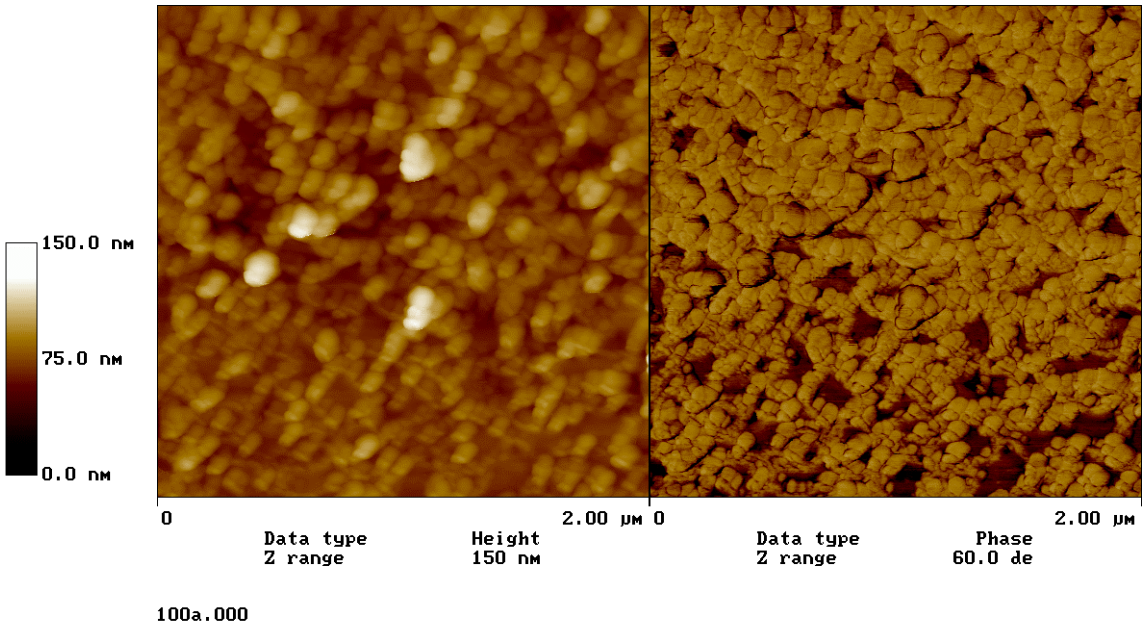

Figure 5.4-11: AFM images of 100t sample.

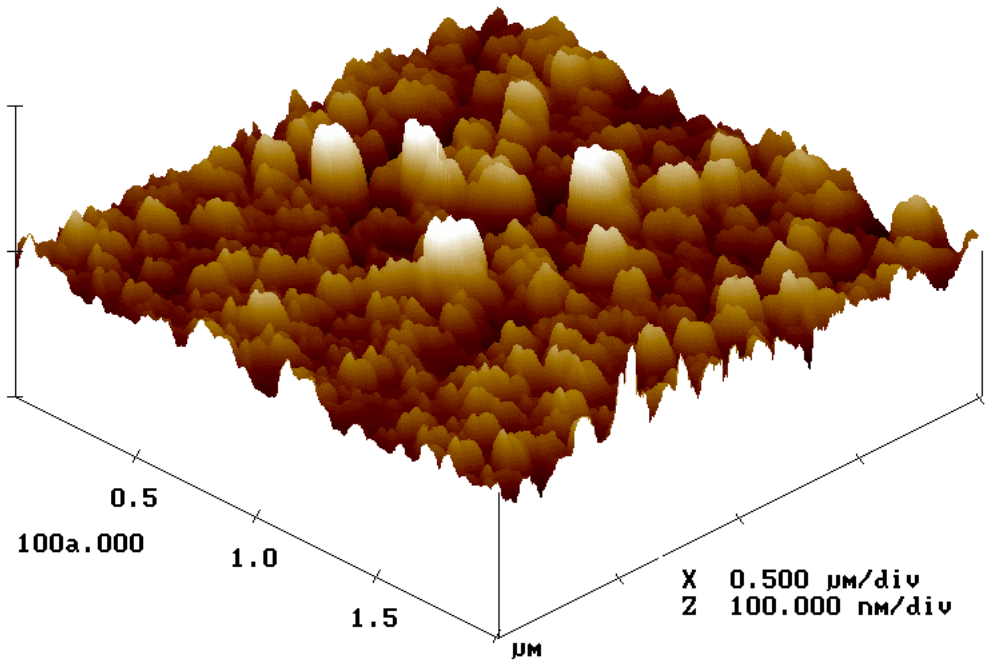

Figure 5.4-12: 3-D AFM image of 100t sample.

AFM images were taken of the hydrolyzed polymer brush samples (Figure 5.4-13 to 5.4-16). These images were compared to the images presented above of the unhydrolyzed samples. Changes in both the morphology and the feature size of the polymer brush samples were noted after hydrolysis. The most obvious difference in morphology was the absence of the worm-like structure in the hydrolyzed samples. The feature size measured for the 40ht sample was appeared less than that of the 40t sample. Likewise, the measurement of the 100ht sample was less than that of the 100t sample.

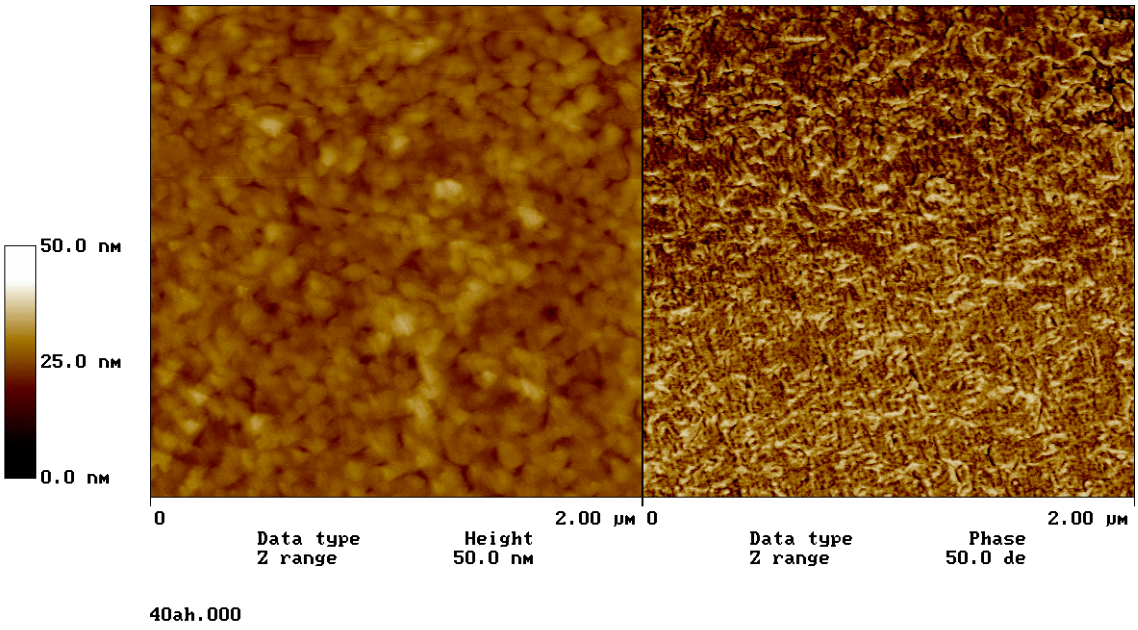

Figure 5.4-13: AFM images of 40ht sample.

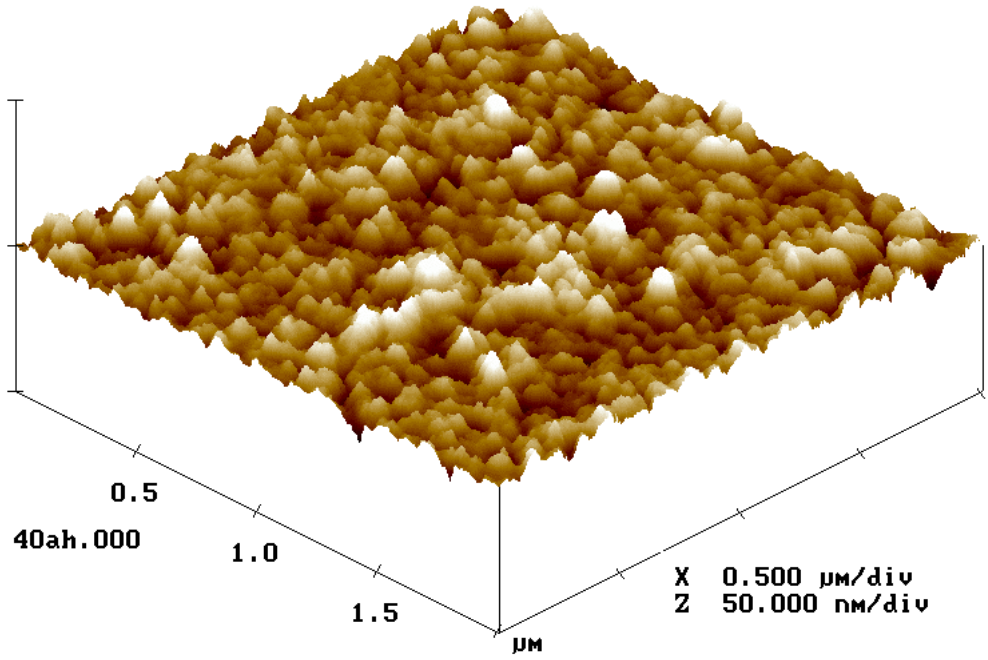

Figure 5.4-14: 3-D AFM image of 40ht sample.

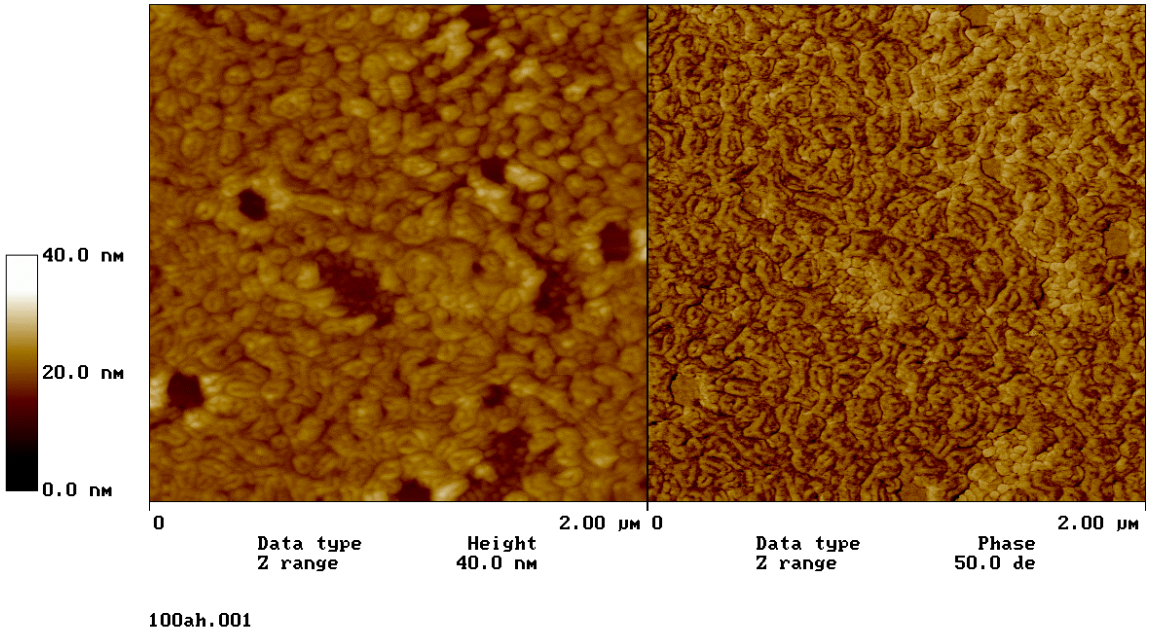

Figure 5.4-15: AFM images of 100ht sample.

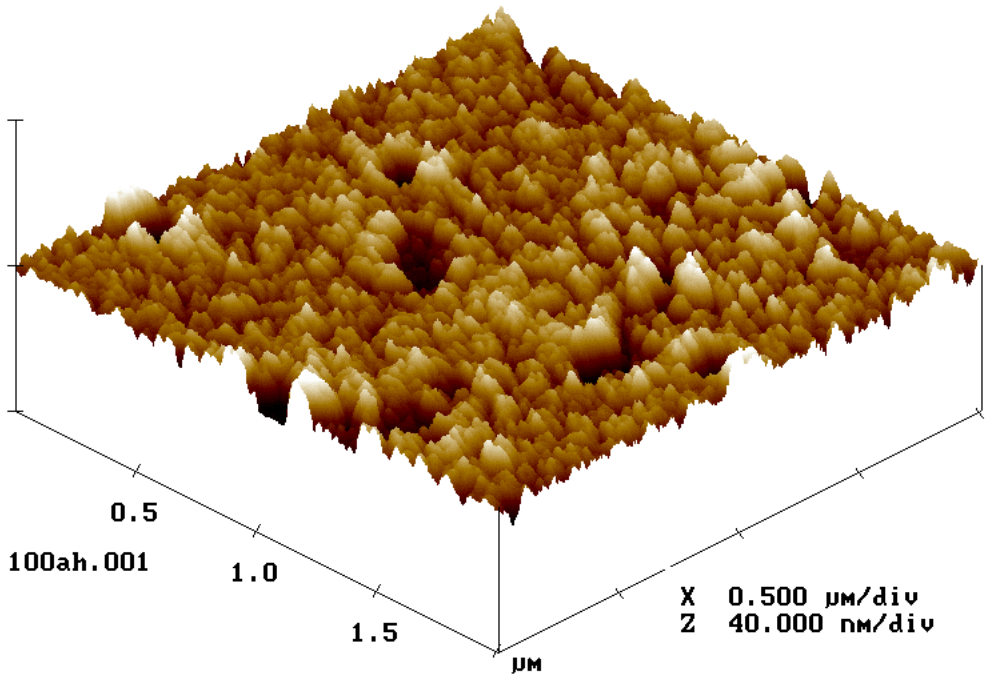

Figure 5.4-16: 3-D AFM image of 100ht sample.

The last AFM images presented are of the polymer brush samples after washing in chloroform. These sample images were compared to those presented above of the 100t and 100ht samples. As shown in Figures 5.4-17 through 5.4-20, chloroform did alter the chain conformations of both the unhydrolyzed and the hydrolyzed samples.

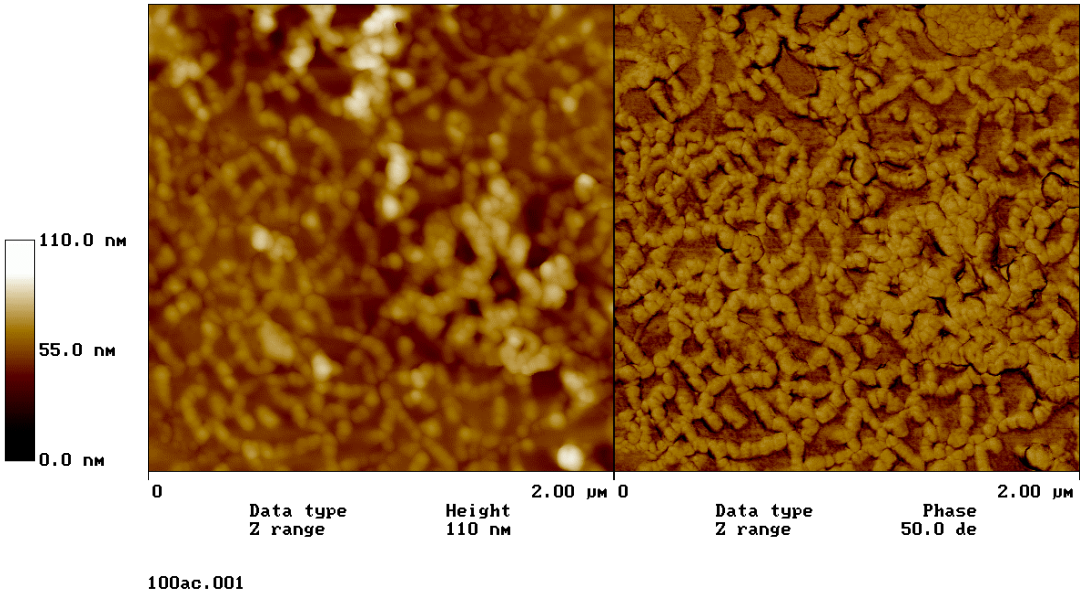

Figure 5.4-17: AFM images of 100c sample.

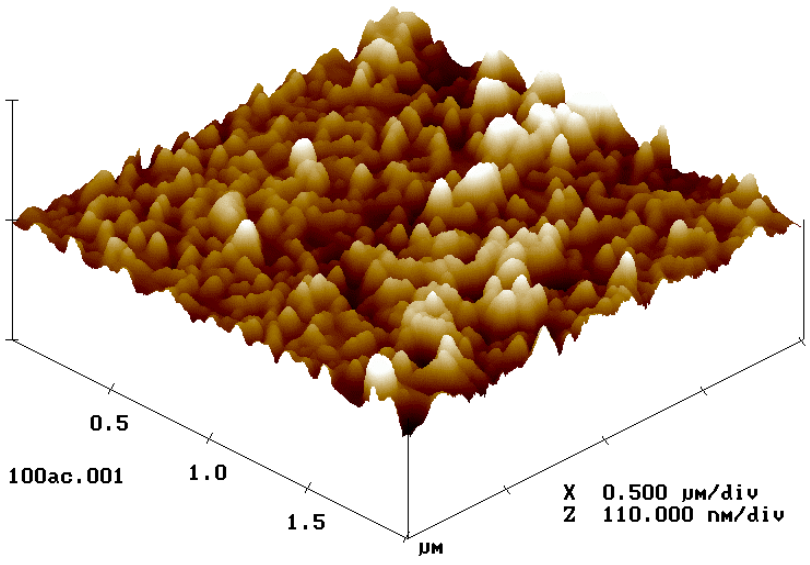

Figure 5.4-18: 3-D AFM image of 100c sample.

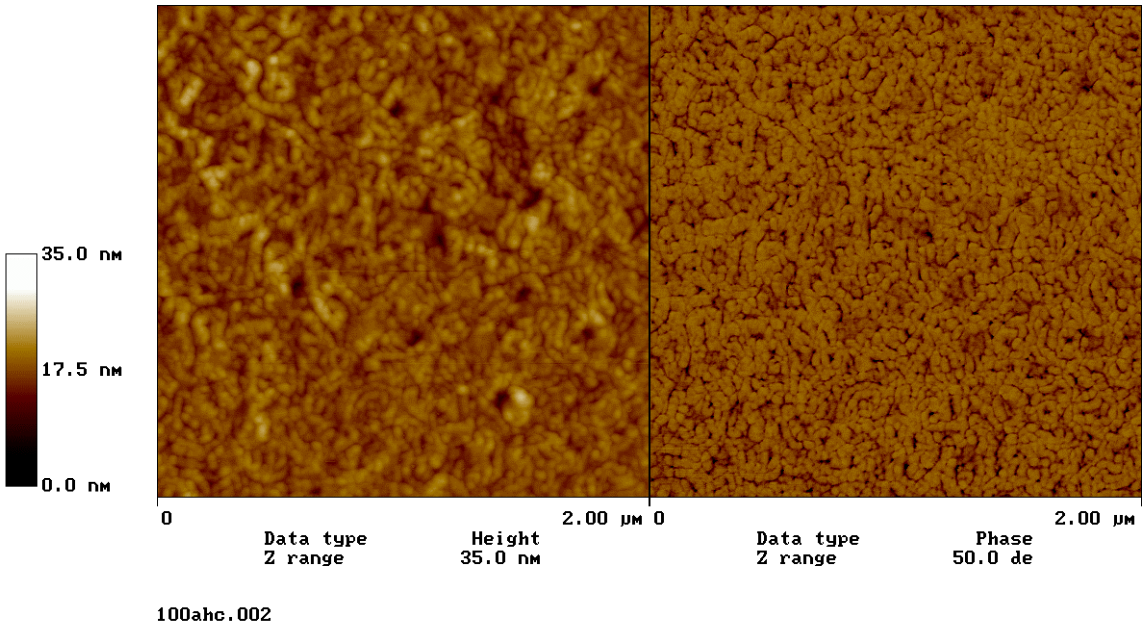

Figure 5.4-19: AFM images of 100hc sample.

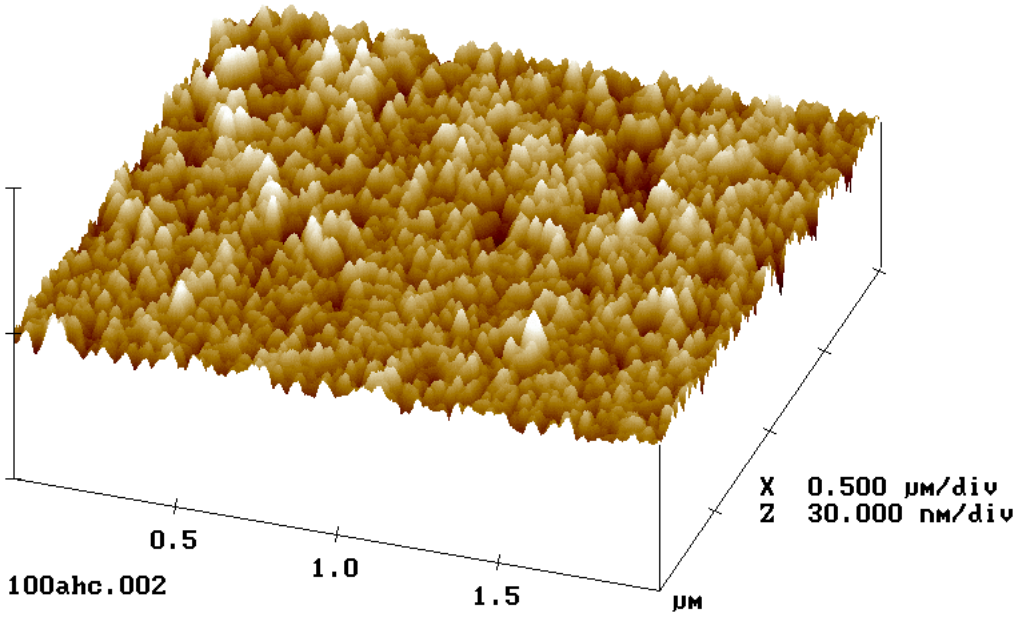

Figure 5.4-20: 3-D AFM image of 100hc sample.

5.4.2 Height Analysis

Height analysis is performed on the AFM. A linear portion of the image is selected. Then, a graphical representation of the height analysis along this line can be presented to the left of the image. Pairs of points on the cross section are designated with arrows and the relative difference in height of the chosen feature is calculated. This value and those of the horizontal distance and surface distance are displayed in a table under the image. It should be noted that this measurement differs from ellipsometry which calculates the total polymer thickness. For each image, at least 6 and as many as 12 height differences have been calculated and averaged together to give an overall feature height of each sample. A summary of the averages is shown in Figure 5.4-21. Individual images and their graphs give a depiction of the typical surface features and more specific measurements.

Height analysis is presented for the 10t, 20t, 40t, and 100t samples (Figure 5.4-21). For these samples a trend relating increasing reaction time and increasing feature height is observed. The height difference increased from 2.55 nm for the 10t sample to 17.53 nm for the 20t sample and then to 24.4 nm for the 40t sample (Figures 5.4-22 to 5.4-24). The 100t sample did decrease slightly in feature height to 19.29 nm seemingly due to inhomogeneous surface features (Figure 5.3-25).

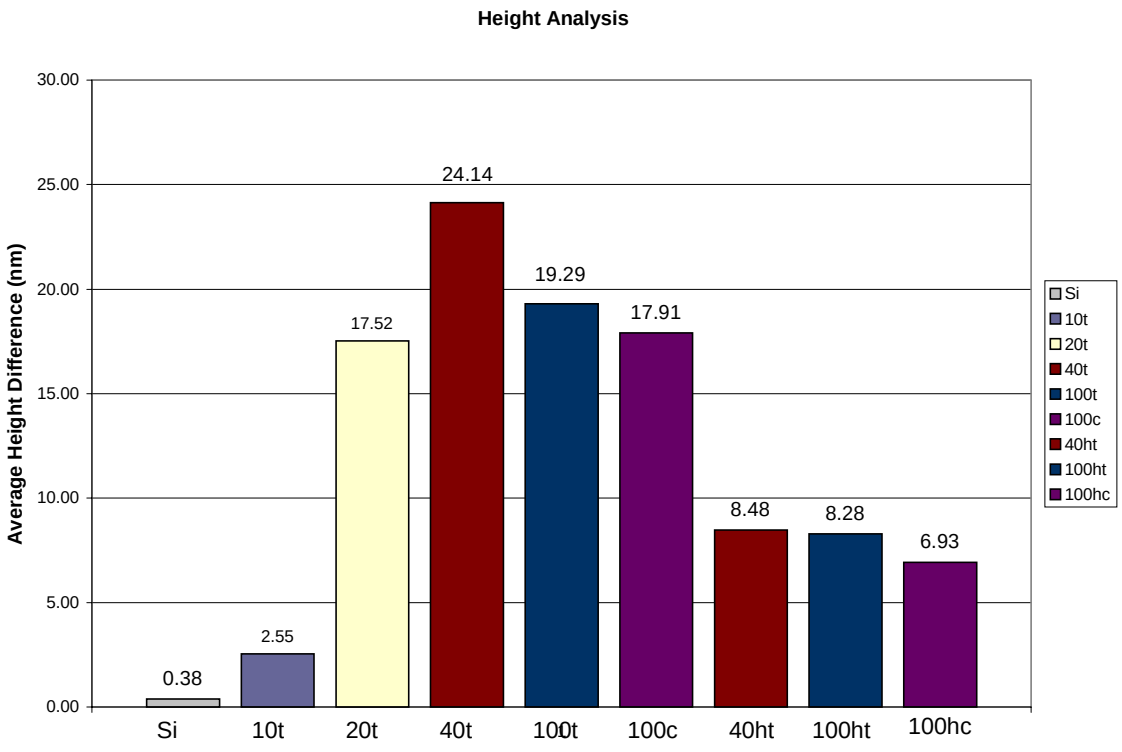

Figure 5.4-21: Summary chart of the average height difference for each polymer brush sample.

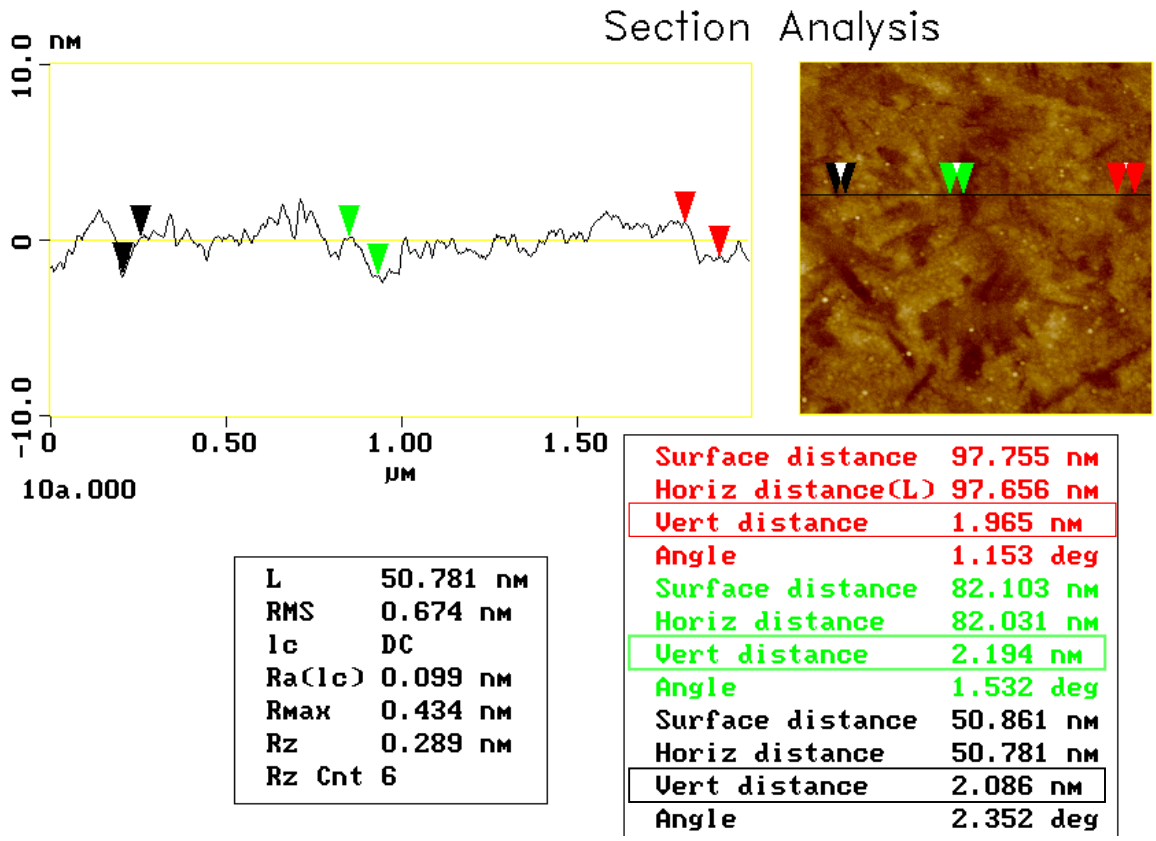

Figure 5.4-22: Height analysis of AFM image for 10t sample.

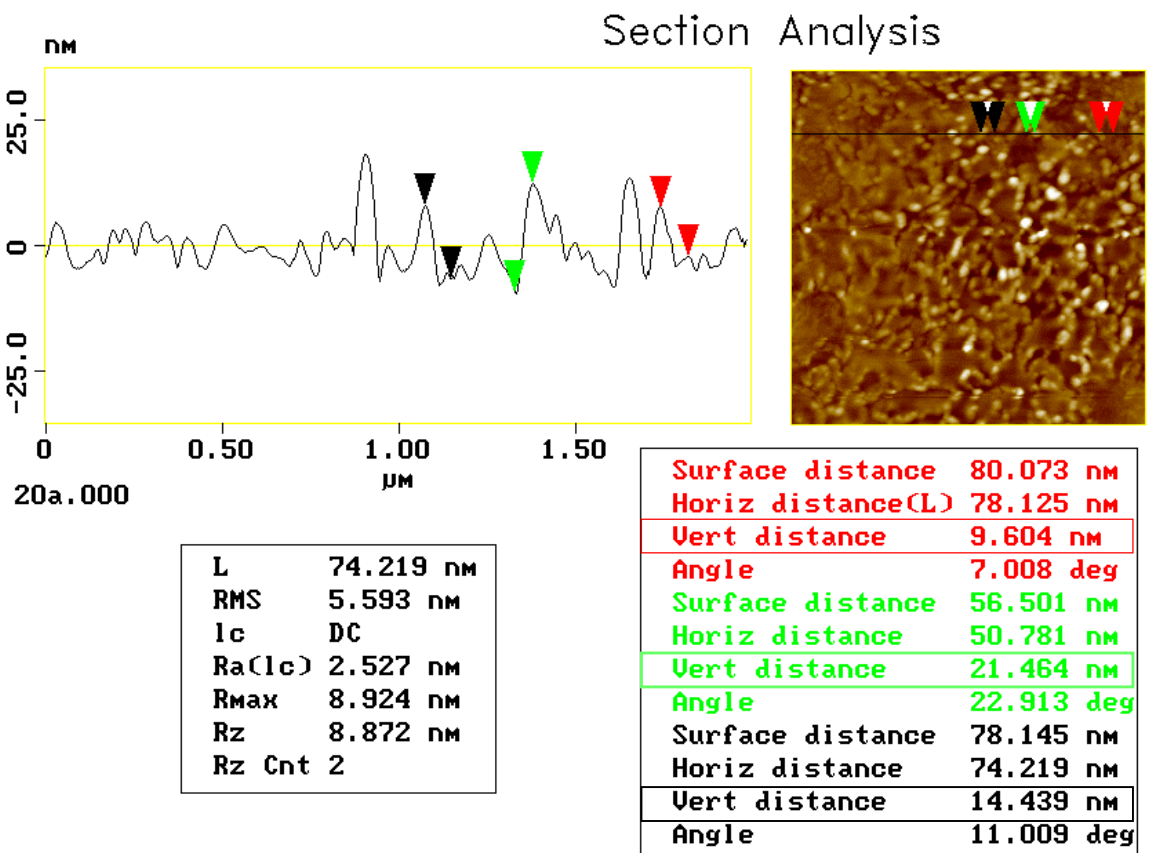

Figure 5.4-23: Height analysis of AFM image for 20t sample.

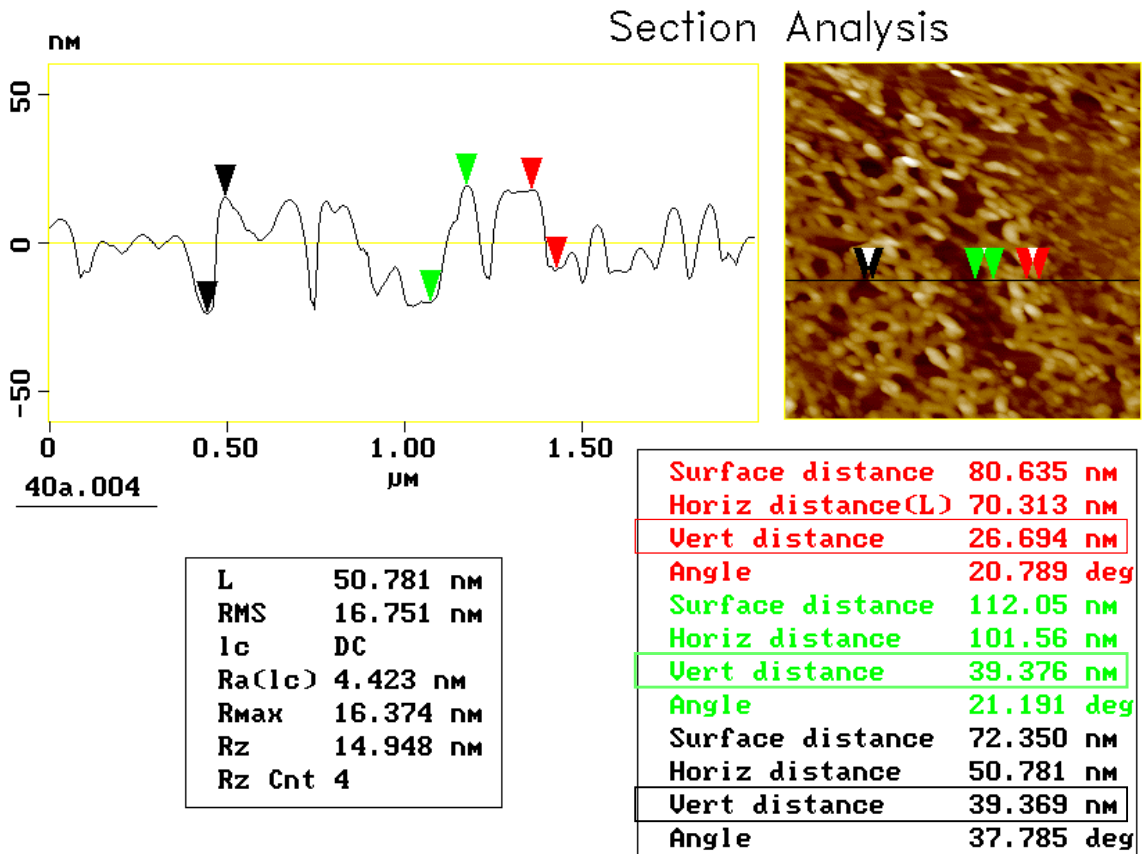

Figure 5.4-24: Height analysis of AFM image for 40t sample.

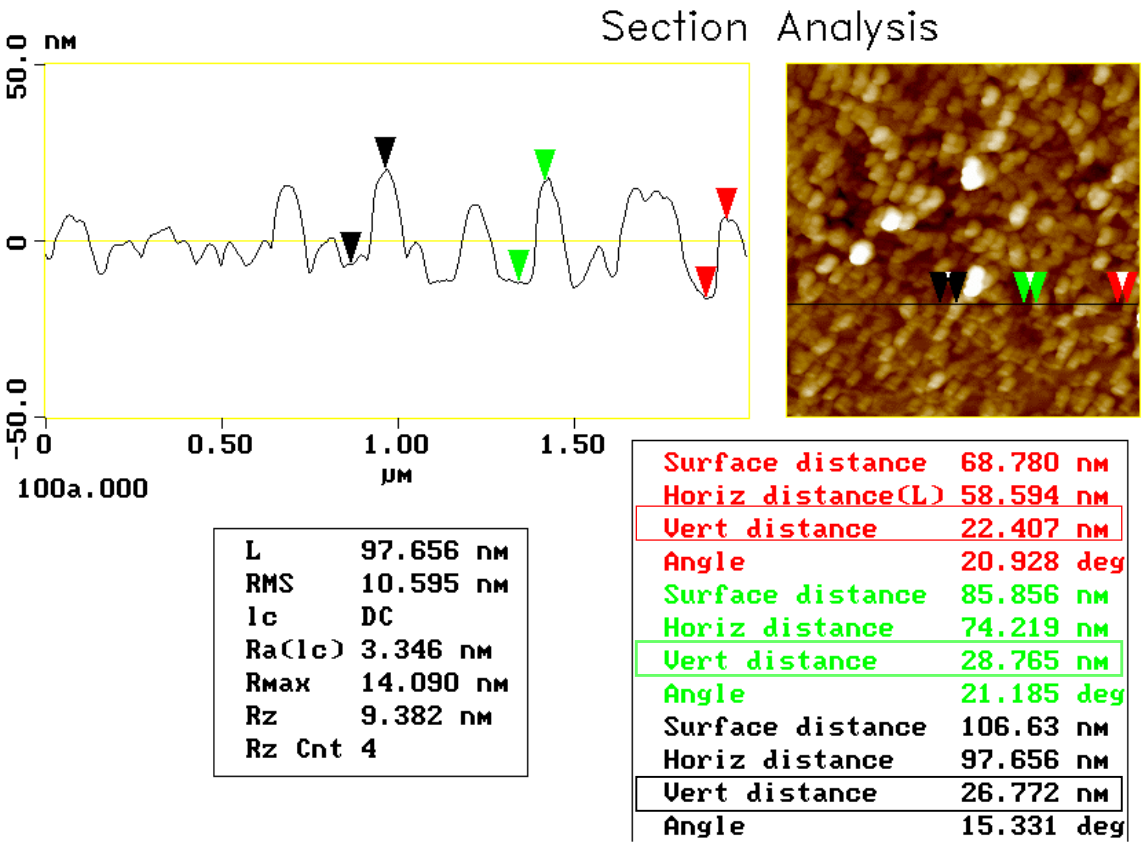

Figure 5.4-25: Height analysis of AFM image for 100t sample.

Height analysis was performed on the 40ht and 100ht samples. The height differences of the features were compared to those of the 40t and 100t samples. The height differences of the hydrolyzed samples decreased in height by 15.66 nm for the 40 hour samples (Figure 5.4-26) and by 11.01 nm for the 100 hour samples (Figure 5.4-27).

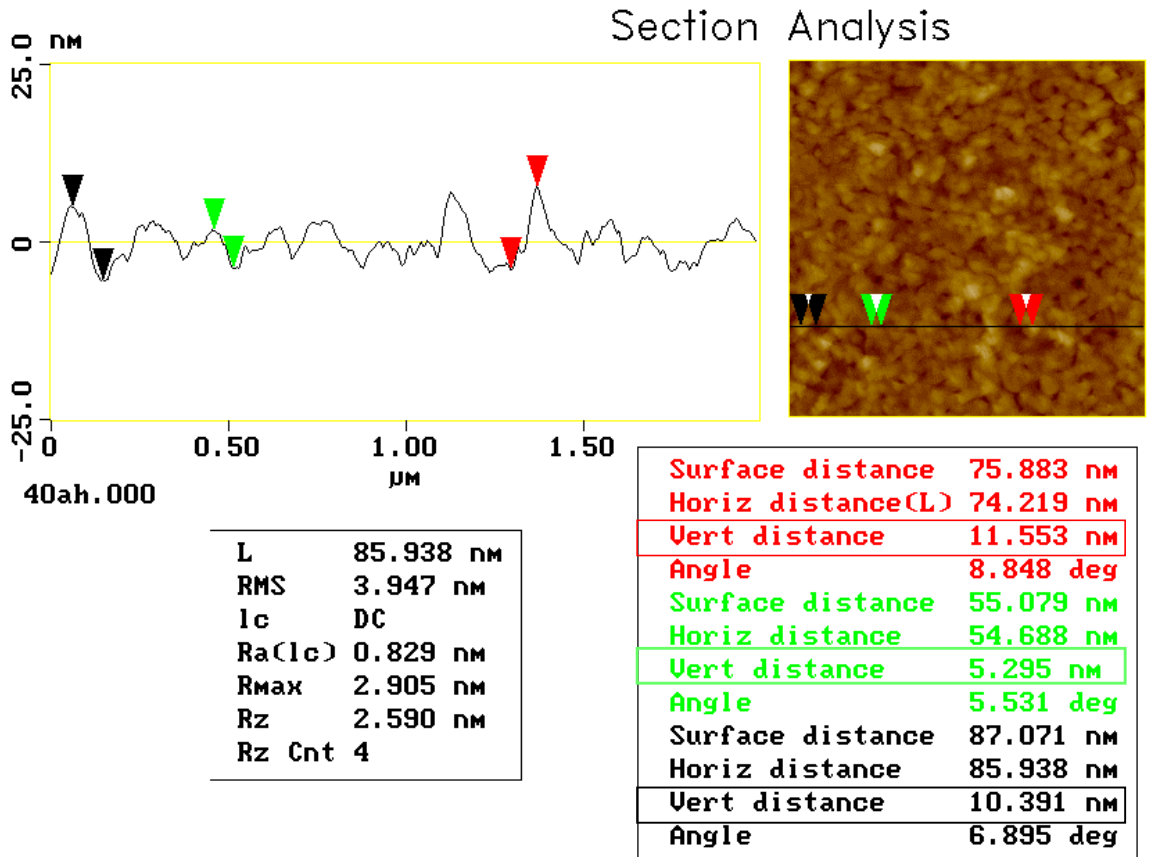

Figure 5.4-26: Height analysis of AFM image for 40ht sample.

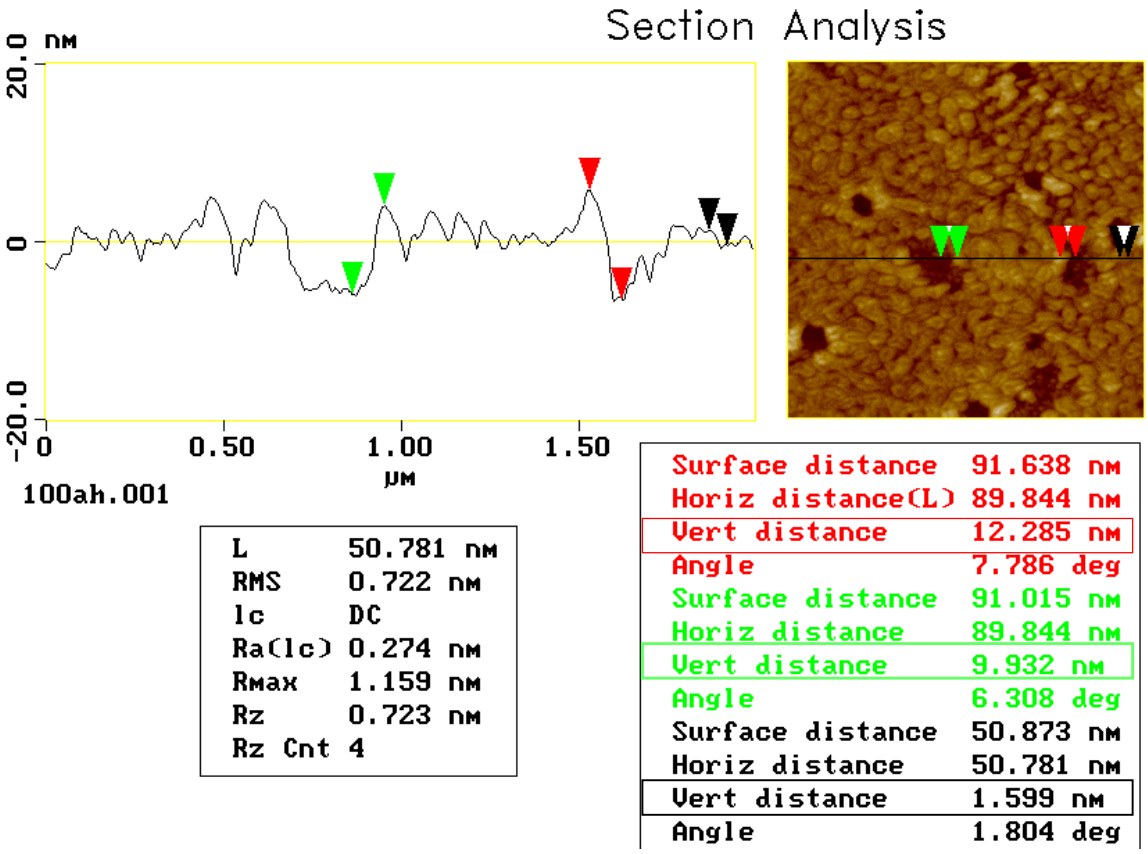

Figure 5.4-27: Height analysis of AFM image for 100ht sample.

Height analysis was also performed for the 100c and 100hc samples. The chloroform wash decreased the feature height difference by 1.38 nm for the 100c sample (Figure 5.4-28) and by 1.35 nm for the 100hc sample (Figure 5.4-29) when compared to the toluene washed samples.

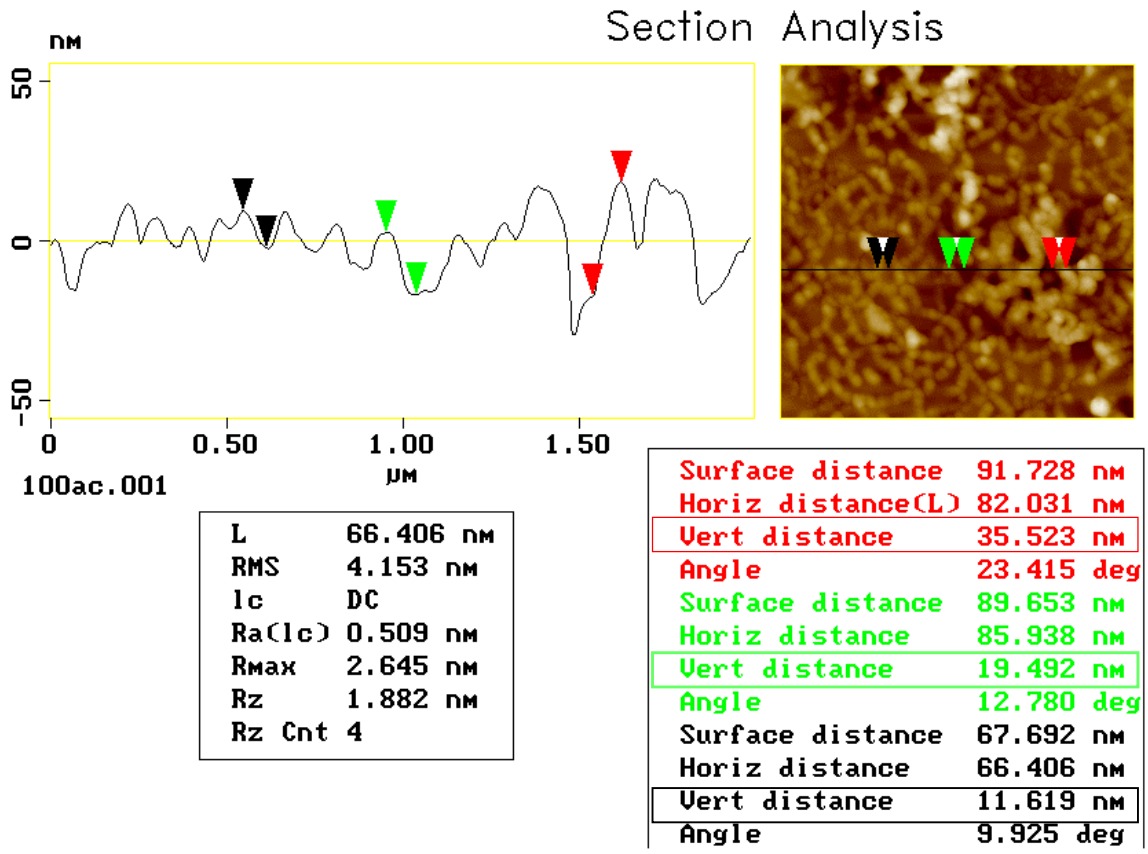

Figure 5.4-28: Height analysis of AFM image for 100c sample.

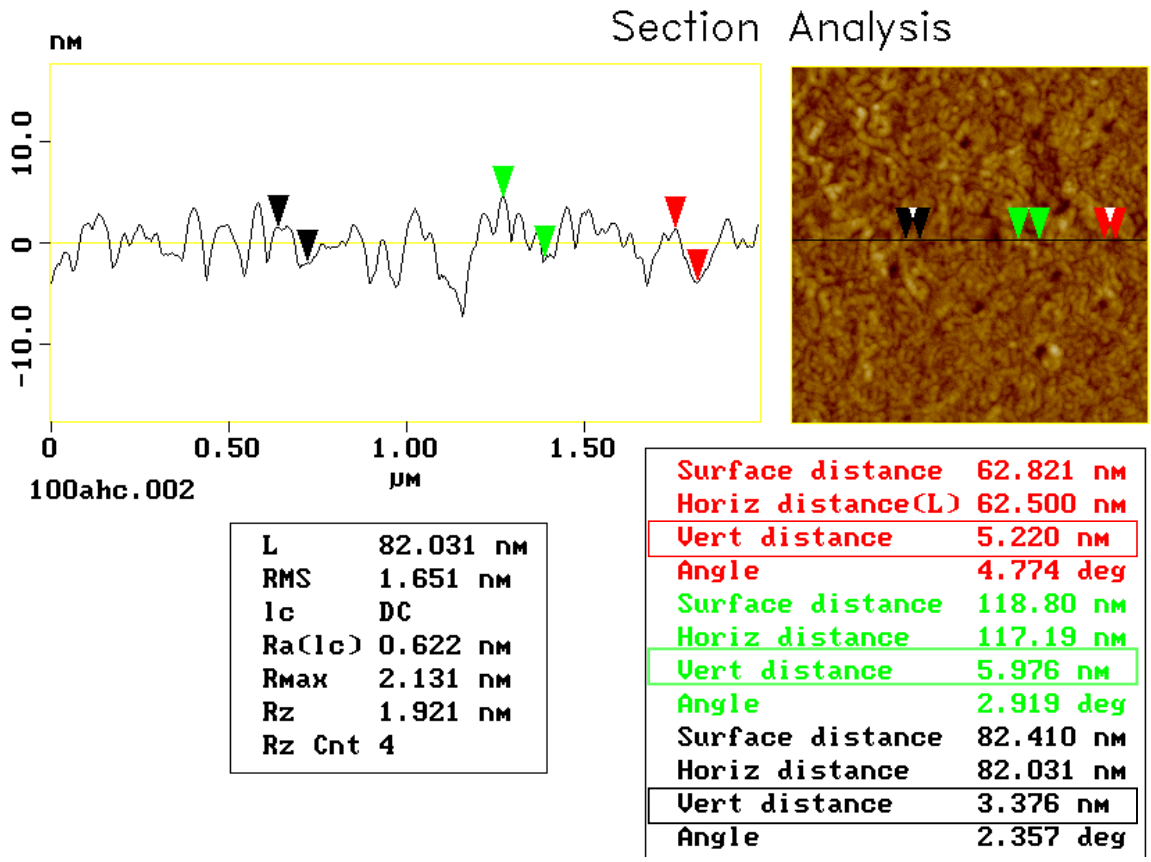

Figure 5.4-29: Height analysis of AFM image for 100hc sample.

5.5 Summary of Polymer Brush Studies

As the initial reaction time was increased, many trends were observed in the polymer brush samples. The first relationship developed was an increase in the contact angle of water, the hydrophobic nature, of the surface as the reaction time increased. Also, an increase in the overall film thickness, as determined by ellipsometry, and an increase in the height, as demonstrated from AFM, measurements provide strong evidence that extending reaction time increases the grafting density of the polymer brush. Also, the AFM images of the series of the 10t, 20t, 40t, and 100t samples showed an increase in the horizontal feature size of the polymer brushes.

The polymer brush samples washed in chloroform were compared to those washed in toluene. The contact angle of water for the 100c sample was less than that of the 100t sample indicating a more polar surface. The AFM images of the toluene washed

and chloroform washed samples strongly indicate different polymer chain conformations. In addition, the height analysis showed a decrease in the height difference for the chloroform samples as compared to that of the toluene samples.

Lastly, the hydrolysis reaction on an existing film was concluded to be successful; both XPS and ellipsometry demonstrated the presence of the polymer brush on the surface. A decrease in the contact angle measurements of water confirmed at least a partial conversion to PMAA. Furthermore, the polar component of the surface energy increased significantly after hydrolysis. However, more work needs to be done to directly relate hydrolysis reaction time to the percent conversion of t-butyl groups. AFM images of the 40ht and 100ht hydrolyzed samples showed a drastic change in morphology with the elimination of the worm-like structure and a decrease in feature size as compared to the 40t and 100t samples. In addition, both ellipsometry and the AFM height analysis of the hydrolyzed samples showed a significant decrease in the film thickness.

References

1. Adam, G., Gibbs, J. H., *J. Chem. Phys*. **1965**, *43*, 139.
2. Angell, C. A., *J. of Non-Cryst. Solids* **1991**, *131-133*, 13-31.
3. Ngai, K. L., Plaxek, D. J., *J. Poly. Sci. Part B: Polymer Physics* **1986**, *24*, 619-632.
4. Ngai, K. L., Roland, C. M., *Macromolecules* **1993**, *26*, (25), 6824-6830.
5. Ngai, K. L., *Journal of Chemical Physics* **1998**, *109*, (16), 6982-6985.
6. Plazek, D. J., Ngai, K. L., *Macromolecules* **1991**, *24*, 1222.
7. *Polymer Handbook*, 3; Brandrup, J., Immergut, E. H., Eds.; John Wiley & Sons, Inc.: NY, 1989; V/79.
8. *New Characterization Techniques for Thin Polymer Films*; Tong, H., Nguyen, L. T., Eds.; John Wiley & Sons, Inc.: NY, 1990.
9. Keddie, J. L., Jones, R. A. L., Cory, R. A., *Faraday Discussion* **1994**, *98*, 219-230.
10. Ngai, K. L., Rizos, A. K., Plazek, D. J., *J. of Non-Cryst. Solids* **1998**, *235-237*, 435-443.
11. Wallace, W. E., van Zanten, J. H., Wu, W. L., *Phys. Rev. E* **1995**, *52*, (4).
12. Van Zanten, J. H., Wallace, W. E., Wu, W., *Phys. Rev. E* **1996**, *55*, (3), R2053-2056.
13. Fryer, D. S., Nealey, P. F., de Pablo, J. J., *Macromolecules* **2000**, *33*, (17), 6439-6447.
14. Porter, C. E., Blum, F. D., *Macromolecules* **2000**, *33*, (19), 7016-7020.
15. Torres, J. A., Nealey, P. F., de Pablo, J. J., *Physics Review Letters* **2000**, *85*, (15), 3221-3224.
16. Hall, D. B., Underhill, P., Torkelson, J. M., *Polymer Engineering and Science* **1998**, *38*, (12).
17. Extrand, C. W., *Polymer Engineering and Science* **1994**, *34*, (5), 390-394.
18. Bornside, D. E., Macosko, C. W., Scriven, L. E., *Journal of Imaging Technology* **1987**, *13*, (4), 122-129.
19. Azzam, R. M. A., Bashara, N. M., *Ellipsometry and Polarized Light*, North-Holland Pub. Co.: NY, 1977.
20. See, V., Cha, J., Chang, T., Ree, M., *Langmuir* **2000**, *16*, 2351-2355.
21. Grosso, D., Balkenende, A. R., Albouy, P. A., Lavergne, M., Mazerolles, L., Babonneau, F., *J. of Materials Chemistry* **2000**, *10*, (9), 2085-2089.
22. *Applied Polymer Analysis and Characterization*; Mitchell, J. Jr., Eds.; Hanser: NY, 1992; 2.
23. Simon, G. P., *Materials Forum* **1994**, *18*, 235-264.
24. Connolly, M., Karasz, F., Trimmer, M., *Macromolecules* **1995**, *28*, 1872-1881.
25. Robertson, C. G., Roland, C. M., *Macromolecules* **2000**, *33*, 1262-1267.
26. Cheremisinoff, N. P. *Polymer Characterization: Laboratory Techniques and Analysis*, Noyes Pubs.: Westwood, NJ, 1996.
27. Jones, R. A. L., Richards, R. W. *Polymers at Surfaces and Interfaces*, Cambridge University Press: United Kingdom, 1999.
28. Milner, S. T., *Science* **1991**, *251* (4996) 905-914.
29. Zhao, B., Brittain, W. J., Zhou, W., Cheng, S. Z. D., *Macromolecules* **2000**, *33*, 8821-8827.
30. Wang, J., Kara, S., Long, T. E., Ward, T. C., *J. of Polymer Science, Part A: Polymer Chemistry* **2000**, *38*, 3742-3750.

31. Wu, S. *Polymer Interface and Adhesion*, Marcel Dekker, Inc.: NY, 1982.
32. Wulf, M., Grundke, K., Kwok, D. Y., Neumann, A. W., *Journal of Applied Polymer Science* **2000**, *77*, 2493-2504.
33. *Polymer Characterization: Physical Techniques*, 2; Campbell, D., Pethrick, R. A., White, J. R., Eds.; Stanley Thornes Ltd.: United Kingdom, 2000.
34. Ngai, K. L., *J. Chem. Phys*. **1998**, *109*, (16), 6982-6985.
35. Zhao, B., Brittain, W. J., *Macromolecules* **2000**, *33*, (2), 342-348.
36. *The Merck Index*, 12; Budavari, S., Eds.; Merck & Co., Inc.: NJ, 1996.
37. TA Instruments Manual for DEA 2970 Dielectric Analyzer
38. Wang, J. to be published.
39. Masky, P., Liu, Y., Huang, E., Russell, T. P., Hawker, C., *Science* 1997, 275, 1458-1460.
40. Digital Instruments Scanning Probe Microscopy Training Notebook
41. Rizos, A. K., Ngai, K. L., *Macromolecules* **1998**, *31*, (18), 6217-6225.
42. Callister, W. D. *Materials Science and Engineering: an Introduction*, 3; John Wiley & Sons, Inc.: NY, 1994.
43. TA Instruments Manual for DMA 2980 Dynamic Mechanical Analyzer

VITA

Catherine Keel Beck was born in April 11, 1977 to Walter and Sandi Keel of Atlanta, Georgia. After graduating from Lassiter High School in 1995, she moved to Blacksburg, Virginia to commence studies at Virginia Tech. She received her Bachelor of Science degree in Chemistry from Virginia Tech in 1999 and married Roger Ezekiel Beck of Mount Vernon, Virginia in August of 2000. She continued her graduate work at Virginia Tech receiving both a Masters of Arts degree in Secondary Science Education and a Masters of Science degree in Polymer Physical Chemistry in 2001. In the fall of 2001, she will begin a position at Narrows High School as their physical science teacher.